



HAL
open science

Microzooplankton diversity and potential role in carbon cycling of contrasting Southern Ocean productivity regimes

Urania Christaki, Ioli-Dimitra Skouroliakou, Alice Delegrange, Solène Irion,
Lucie Courcot, Ludwig Jardillier, Ingrid Sassenhagen

► To cite this version:

Urania Christaki, Ioli-Dimitra Skouroliakou, Alice Delegrange, Solène Irion, Lucie Courcot, et al.. Microzooplankton diversity and potential role in carbon cycling of contrasting Southern Ocean productivity regimes. *Journal of Marine Systems*, 2021, 219, pp.103531. 10.1016/j.jmarsys.2021.103531 . insu-03664866

HAL Id: insu-03664866

<https://insu.hal.science/insu-03664866v1>

Submitted on 24 Apr 2023

HAL is a multi-disciplinary open access archive for the deposit and dissemination of scientific research documents, whether they are published or not. The documents may come from teaching and research institutions in France or abroad, or from public or private research centers.

L'archive ouverte pluridisciplinaire **HAL**, est destinée au dépôt et à la diffusion de documents scientifiques de niveau recherche, publiés ou non, émanant des établissements d'enseignement et de recherche français ou étrangers, des laboratoires publics ou privés.



Distributed under a Creative Commons Attribution - NonCommercial 4.0 International License

22 ABSTRACT

23 Microzooplankton play an important role in aquatic food webs through their multiple interactions
24 with other organisms and their impact on carbon export. They are major predators of phytoplankton
25 and bacteria while being preyed on by higher trophic levels. Microzooplankton diversity
26 (Dinoflagellates, DIN and Ciliates, CIL), community structure, interaction with phytoplankton and its
27 potential in channeling carbon to higher trophic levels were studied in contrasting productivity
28 regimes (off- and on-plateau, the latter been naturally fertilized by iron) around the Kerguelen islands
29 in the Southern Ocean (SO). DIN and CIL diversity was sampled in late summer (February-March
30 2018; project MOBYDICK) and at the onset-of the bloom (KEOPS2 cruise), and assessed by
31 Illumina sequencing of 18S rDNA amplicons and microscopic observations. The diversity obtained
32 by the two approaches could be compared at a relatively high taxonomic level (i.e., often to family
33 level). In particular for DIN, relative abundances and ranking of dominant taxa differed between
34 sequencing and microscopy observations. CIL were always recorded at considerably lower
35 abundances than DIN, the median of their abundances across stations and seasons being 350 and
36 1370 cells L⁻¹, respectively. During late summer, DIN and CIL biomasses were about 1.5 times
37 higher on- than in off-plateau waters, while community composition was spatially similar. The most
38 abundant DIN at all stations and during both seasons were small *Gymnodinium* (<20µm). During late
39 summer, ciliates *Lohmaniella oviformis* (<20µm) and *Cymatocylis antarctica* (20-40µm) dominated
40 on- and off-plateau, respectively. Dilution experiments suggested significant grazing of
41 microzooplankton on phytoplankton as phytoplankton net growth (k) was lower than
42 microzooplankton grazing (g) at all stations (mean k= 0.16±0.05 d⁻¹, g=0.36±0.09 d⁻¹) in late summer.
43 Despite having great potential as a phytoplankton grazer, microzooplankton occurred at low biomass
44 and showed little temporal variability, suggesting that they were controlled by copepod predation.
45 Microzooplankton are a key component of the SO as an intermediate trophic level mediating carbon
46 transfer from primary producers to higher trophic levels.

47

48 **Keywords:** dinoflagellates; ciliates; microscopy, metabarcoding, dilution experiments, Southern
49 Ocean

50

51 1. Introduction

52 Dinoflagellates (DIN) and ciliates (CIL) represent the most abundant microzooplankton groups in
53 planktonic food webs, where they play a pivotal role as phytoplankton consumers, food source for
54 mesozooplankton and contributors to nutrient remineralization (e.g., Calbet and Landry 2004;
55 Irigoien et al. 2005; Sherr and Sherr 2007; 2009, Caron and Hutchins 2013; Steinberg and Landry
56 2017 and references therein). The proportion of carbon produced by the phytoplankton that is
57 ingested by microzooplankton is highly variable and can exceed mesozooplankton consumption (e.g.,
58 Calbet and Landry 2004, Schmoker et al. 2013; Menden-Deuer et al. 2018). Microzooplankton is
59 able to closely track phytoplankton temporal dynamics because they overall share similar growth
60 rates. Blooms, thus occur when particular phytoplankton taxa successfully escape microzooplankton
61 control (Irigoien et al. 2005; Sherr and Sherr, 2009). At a global scale, predatory protists and
62 phytoplankton biomass display a curvilinear relationship and the plateau observed at about 50 $\mu\text{g C}$
63 L^{-1} for phytoplankton has been attributed to predation by mesozooplankton (Irigoien et al. 2005). In
64 fact, mesozooplankton preferentially grazes on microzooplankton (e.g., Stoecker and Capuzzo 1990;
65 Kiorboe and Wisser 1999; Calbet and Saiz, 2005; Vargas and Gonzalez 2004; Campbell et al. 2009;
66 Sherr and Sherr 2009), releasing predation pressure on phytoplankton and favoring its blooming
67 capacity (e.g., Grattepanche et al. 2011a). Due to the central position of microzooplankton in aquatic
68 food webs and the direct interaction with primary producers, any change in community structure and
69 activity can have marked implications for multiple trophic levels and carbon export. Such changes in
70 carbon export are expected in the future, as modeling studies suggest that ocean warming will
71 enhance loss of primary production to microzooplankton herbivory in chlorophyll rich waters (Chen
72 et al. 2012). Trophic transfer of carbon produced by phytoplankton through microzooplankton rather
73 than directly via mesozooplankton predation would result in lower C-export (Hall and Safi 2001;
74 Smetacek et al. 2004). Despite several centuries of studies on protists, untangling the impact on
75 carbon transfer of heterotrophic protists in plankton communities remains challenging due to their
76 fragility, lack of direct methods to accurately measure their growth rate, and time-consuming
77 identification and counting (reviewed in Caron et al. 2009; 2012; Caron and Hutchins 2013)

78 In the Southern Ocean (SO), diatoms and haptophytes are usually identified as the major primary
79 producers and their diversity and role in the C-cycle have been described in detail in previous studies
80 (e.g., Smetacek et al. 2004; Poulton et al. 2007; Armand et al. 2008; Queguiner 2013; Wolf et al.
81 2014, Lasbleiz et al. 2016, Irion et al. 2020 among many others). By contrast, microbial heterotrophs
82 and, in particular, phytoplankton predators, have been far less investigated (Caron et al. 2000; Hall
83 and Safi 2001; Saito et al. 2005; HENZES et al. 2007; Christaki et al. 2008; Poulton 2007, Christaki et

84 al. 2015; Morison and Menden-Deuer 2018 and references therein). In the SO, Kerguelen and Crozet
85 islands are characterized by iron enrichment of surface waters. This results in large phytoplankton
86 blooms in these waters that contrast with the surrounding HNLC (High Nutrients Low Chlorophyll)
87 conditions (Blain et al. 2007; Pollard et al. 2007, 2009). The rare studies that have provided
88 information on microzooplankton community structure in the Crozet and Kerguelen areas reported a
89 prevalence of DIN over CIL biomass (Poulton 2007, Christaki et al. 2015). Microzooplankton were
90 identified as a major consumer of phytoplankton during the onset and decline of Kerguelen blooms
91 (Brussaard et al. 2008; Christaki et al. 2015) and an important player in iron regeneration (Sarhou et
92 al. 2008).

93 The present study was realized in the framework of the MOBYDICK project (Marine Ecosystem
94 Biodiversity and Dynamics of Carbon around Kerguelen: an integrated view). MOBYDICK's aim
95 was to trace C from its biological fixation and cycling within and across trophic levels at surface, as
96 well as its export to depth under different productivity regimes of the Southern Ocean after the
97 phytoplankton bloom, in late summer. The objective of this study was to provide information about
98 the diversity and the community structure of microzooplankton (DIN and CIL) in relation to
99 phytoplankton communities and to estimate their potential capacity for channeling carbon to higher
100 trophic levels. The results obtained during the post-bloom period (MOBYDICK cruise) are discussed
101 here along with observations from the onset of a previous bloom (KEOPS2 cruise).

102 2. Material and Methods

103 2.1 Study site, Sample collection

104 The MOBYDICK cruise took place during the late Austral summer (from 19 February to 20 March
105 2018), where samples were collected at four stations (M1, M2, M3, and M4. Figure 1). Station M2,
106 above the Kerguelen plateau, was located in naturally iron-fertilized waters (Blain et al. 2007),
107 characterized by intense phytoplankton blooms during spring and summer (Moserri et al. 2008;
108 Cavagna et al. 2014). Stations M1, M3, and M4, situated off-plateau, were in an oceanic area of
109 HNLC (High-nutrient, low-chlorophyll) waters (Cavagna et al. 2015). The sampling strategy
110 included repeated visits at the different stations. Station M2 was sampled three-times at eight day
111 intervals (M2-1, M2-2, and M2-3); stations M3 and M4 were sampled twice with two-week intervals
112 (M3-1, M3-3, M4-1, and M4-2); and station M1 was sampled just once (Table 1). Samples were
113 collected with 12L Niskin bottles mounted on a rosette equipped with CTD (SeaBird 911-plus).

114 Pigments were analyzed using High Performance Liquid Chromatography (HPLC, Ras et al. 2008).
115 CHEMTAX analysis was performed with CHEMTAX v1.95 (Mackey et al. 1996) to estimate the

116 pigment:Chl *a* ratios for seven major phytoplanktonic groups: chlorophytes, prasinophytes,
117 cyanobacteria, cryptophytes, diatoms, dinoflagellates, and haptophytes (detailed in Irion et al. 2020).
118 Pigments and microzooplankton data (see below) from the onset of the bloom (early spring, October-
119 November 2011, KEOPS2 cruise, Georges et al. 2014, Christaki et al. 2015) were included here for
120 comparison with post-bloom MOBYDICK period (this study); KEOPS2 pigments were analyzed
121 with CHEMTAX as described above.

122

123 2.2 Molecular analysis

124 Water samples were collected at all stations (M1, M2, M3, and M4) at four depths (15 m, 60 m,
125 125 m, and 300 m). The depths were chosen to correspond to the surface and the bottom of the mixed
126 layer (ML), the transition between surface and deeper waters (125 m), and the deep nutrient rich
127 waters (300m). After pre-filtering through 100µm mesh to remove most of the metazoans, ten liters of
128 seawater from each depth were filtered successively through 20µm and 0.2µm using a peristaltic
129 pump ('large' and 'small' size fractions, respectively). Filters were stored at -80°C until DNA
130 extraction. The extraction, PCR procedure, and downstream analysis are described in detail in
131 Sassenhagen et al. (2020). Briefly, extraction was realized with PowerSoil DNA Isolation Kit
132 (QIAGEN, Germany) following standard manufacturer's protocol. The 18S rDNA V4 region was
133 amplified using EK-565F (5'-GCAGTTAAAAAGCTCGTAGT) and UNonMet (5'-
134 TTTAAGTTTCAGCCTTGCG) primers (Bower et al. 2004). Libraries were paired-end (2 x 300bp)
135 Illumina MiSeq sequenced. The forward and reverse reads were demultiplexed using Qiime1 pipeline
136 (Caporaso et al. 2010). The reads were further trimmed and filtered in the *R*-package DADA2
137 (Callahan et al. 2016). The same package was used for identification of amplicon sequencing variants
138 (ASV) and their taxonomical assignment based on the PR² database (Guillou et al. 2013). ASVs
139 affiliated to Metazoa, Streptophyta, as well as rare ones with less than 15 reads in the whole data set,
140 were removed with the *R*-package 'phyloseq' (McMurdie and Holmes 2013).

141 To investigate the phylogenetic relationship between the observed genera, the sequences generated in
142 this study and additional sequences from the Genbank database were aligned using the software
143 muscle 3.8.31 (Edgar, 2004) with default settings. The alignments were trimmed with the software
144 trimAl v1.2 (Capella-Gutiérrez et al. 2009) applying a gap threshold of 0.6. Maximum likelihood
145 trees were separately build for DIN and CIL with the software RAxML version 8.2.12 (Stamatakis,
146 2014) using the substitution model "GTRCAT". The RAxML settings included rapid bootstrap
147 analysis, while the number of distinct starting trees was based on bootstrapping criteria. The tree was
148 visualized with the online application iTOL (Letunic and Bork, 2016).

149

150 2.3 Microscopic analysis

151 At each station, microzooplankton samples were taken from 10 to 12 depths between the surface and
152 300m. Sample volume was 500ml from surface to 200m, and 1L at 300m. Samples were fixed with
153 acid Lugol's solution (2% v/v). All samples were kept at 4°C in the dark until microscopy analysis.
154 In the laboratory, samples were left to settle in graduated cylinders for four days, then the 100 ml
155 bottom of each sample was transferred into settling chambers and left to settle for another 24h before
156 examination under an inverted microscope (Nikon Eclipse TE2000-S; x400). DIN and CIL were
157 identified based on their morphology at the lowest possible taxonomic level following (Tomas, 1997;
158 McMinn and Scot 2005; Kofoid and Campbell, 1929; Schiller, 1931-1937; Petz, 2005; Georges et al.
159 2014). DIN and CIL were also classified into six size classes (<20, 20–40, 40–60, 60–80, 80–100,
160 and >100 µm). Linear dimensions were measured at x400 magnification using an image analyzer
161 with a camera mounted on the microscope. Biovolume measurements were converted into biomass
162 using a conversion factor of 190 fg C µm⁻³ (Putt and Stoecker, 1989) and 0.760 x volume^{0.819} pg C
163 µm⁻³, respectively (Menden-Deuer and Lessard 2000).

164 2.4 Microzooplankton herbivory via dilution experiments

165 Dilution experiments were conducted at all stations following the protocol of Landry and Hassett
166 (1982). However, due to a change in shipboard operational procedure at station M3-3, a significant
167 increase in incubator water temperature occurred. Although samples were analyzed, (phytoplankton
168 growth almost doubled while grazing remained of the same levels) the results are not presented here.
169 Fifty liters of subsurface seawater, representative of the mixed layer, were collected at 30 m depth
170 with Niskin bottles and gently screened through a 200µm sieve to remove metazoans. Twenty liters
171 of 0.2 µm filtered seawater (FSW) were prepared through low-pressure filtration (<50 mm Hg). Five
172 different concentrations (10%, 25%, 50%, 75%, and 100%) were prepared by mixing <200µm and
173 <0.2µm filtered seawater. For each treatment, three 2.4L polycarbonate bottles were filled to the rim
174 by gently siphoning from the carboys. Light measurements prior to incubation indicated that 25%
175 light was available between 19 and 35m (average: 25 ±6m) which matched with the sampling depth
176 (30m) for the dilution experiment. Thus, 25% light was the best compromise between experimental
177 constraints and field measurements. All 15 bottles were incubated for 24h in an on-deck incubator
178 connected to the flow-through sea surface-water system and covered with a lid that let 25% of PAR
179 light through (equivalent light condition to *in situ* surface waters). Additionally, 2.4L were set aside
180 for immediate sampling at T0. For Chl *a* measurement at the end of the incubation, 500-700 ml from

181 each bottle were filtered onto 0.2 μm polycarbonate filters (ϕ 47 mm). After filtration, each filter was
182 placed into 2 ml cryotubes, flash frozen in liquid nitrogen and stored at -80°C . Chl *a* concentrations
183 were estimated by fluorometry (Lorenzen, 1966). Filters were extracted overnight in 90% acetone at
184 4°C . At the end of the extraction period, Chl *a* concentration was determined using a calibrated
185 Turner Trilogy[©] fluorometer. Initial Chl *a* concentration for each dilution treatment was estimated by
186 multiplying initial whole seawater Chl *a* concentrations by corresponding dilution factors. Assuming
187 a phytoplankton exponential growth, changes in Chl *a* concentration over the experiment were used
188 to calculate the instantaneous phytoplankton growth (k , d^{-1}), and grazing mortality (g , d^{-1} , Landry and
189 Hasset 1982, Figure A1). Grazing pressure ($\%$ Chl *a* production d^{-1}) has been calculated as the ratio
190 between phytoplankton daily production ($\mu\text{g Chl a L}^{-1} \text{d}^{-1}$) and microzooplankton daily consumption
191 ($\mu\text{g Chl a L}^{-1} \text{d}^{-1}$).

192 2.5 Data analysis

193 Co-inertia analysis (PCA-PCA COIA) was used to investigate the coupling between phytoplankton
194 pigments and CIL and DIN communities (Dolédéc and Chessel 1994, Dray et al. 2003). The
195 abundances obtained through microscopic counts of the 16 most abundant genera (8 DIN and 8 CIL),
196 representing $>90\%$ of total abundance at each station were used. COIA differs from other 'classic'
197 canonical models in utilizing partial least-squares regression, rather than multiple regression, to
198 summarize common structure. Because COIA is based on partial least-squares regression, it places no
199 restrictions on the number of variables that can be analyzed (unlike the classic canonical models).
200 The co-inertia model is symmetric, and therefore descriptive rather than predictive (for more details
201 Kenkel 2006). COIA defines axes that simultaneously explain the highest possible variance in each
202 of the two matrices and describes their closest possible common structure. In a 'PCA-PCA COIA' as
203 applied here, a PCA (principal component analysis) was performed on each matrix prior to applying
204 a COIA analysis.

205 A PCA (principal component analysis) was performed on each matrix prior to applying a COIA
206 analysis (Dray et al. 2003). For PCA analysis, variables were standardized and PCA was performed
207 using the R-package FactoMineR (Lê et al. 2008). COIA was carried out with the 'ade4' package in
208 R-software (Dray and Dufour 2007). The strength of the coupling between the two matrices, in
209 COIA is expressed by the multidimensional correlation coefficient (RV), and statistical significance
210 was tested using a Monte Carlo permutation procedure with 1000 permutations. Finally, in order to
211 define the variables that were the most important in structuring the COIA scatterplot, Pearson's
212 correlation coefficients were calculated between all variables and COIA coordinates. All statistical

213 analyses were based on abundances from microscopical counts to avoid the biases of the sequencing
214 data (see results and discussion sections).

215

216 3. Results

217 3.1 Environmental Conditions and Phytoplankton composition

218 The four stations sampled during MOBYDICK were situated in different hydrological conditions.
219 Station M1, which was situated in Antarctic waters and influenced by the polar front, was
220 characterized by a shallow Z_{ML} (27 m, Table 1, Figs. 1 and 2). Stations M2 and M4, which were
221 situated south of the polar front in Antarctic waters, presented a characteristic temperature minimum
222 at 200m and showed the lowest surface temperature (at M4: 4.5°C) (Table 1, Figs. 1 and 2). Station
223 M3, which was situated in sub-Antarctic waters (SAZ), showed the highest temperature in the ML
224 (5.6° C, Table 1). The Z_{ML} deepened at all stations following a storm on the 10th of March 2018.
225 Phosphate and nitrate concentrations were high at all stations while silicic acid was overall higher
226 off-plateau (Table 1). For comparison with early spring (KEOPS2 cruise), stations A3 (on-plateau)
227 and R (defined as the reference station off-plateau) are also shown in Fig. 1 and Table 1. Briefly, A3-
228 1 was sampled in late October, just before the initiation of the bloom. A3-2 was explored about 3.5
229 weeks later, during the onset of the bloom. During early spring, the Z_{ML} at these stations was >100m
230 (Table 1, Christaki et al. 2014) . During MOBYDICK, Chl a in the Z_{ML} doubled between the first and
231 the third visit at M2 (from 0.27 to 0.58 $\mu\text{g L}^{-1}$). Chl a at the off-plateau stations ranged between 0.14
232 and 0.35 (M3-3 and M1, respectively (Table 1, Fig. 1). The concentrations of group pigment
233 signatures analyzed with CHEMTAX illustrated the phytoplankton community structure. Diatoms
234 and prymnesiophytes were always the two major groups. Their respective proportions varied between
235 seasons (early spring or late summer) and positions (on- or off-plateau). Diatoms were dominating
236 during early spring (74-94% of total Chl a in on-plateau water; Fig. 3a, b) while Prymnesiophytes
237 were the most abundant phytoplankton group during late summer (37-53% and 59-70% of total Chl a
238 in on- and off-plateau, respectively ; Fig. 3a, b). The third group contributing most to the
239 phytoplankton biomass were pico- planktonic Prasinophytes that accounted for up to 21 % of Chl a
240 during early spring in HNLC waters (R-2) and up-to 16.5 % of Chl a on the plateau during late
241 summer (M2-3).

242 3.2 Microzooplankton communities

243 3.2.1. Abundance, biomass distributions and morphological diversity

244 During MOBYDICK, microscopy observations allowed the identification, size measurement, and
245 biomass estimation of dinoflagellates (DIN) and ciliates (CIL) (Fig. 4 a-f). Mean integrated
246 abundance in the mixed layer showed that DIN were from 3 to 6 fold more abundant than CIL in the
247 ML and varied between 0.29 and 2.3×10^3 and 0.28 to 0.45×10^3 cells L^{-1} for DIN and CIL,
248 respectively (Fig. 4 a, c). During late summer, DIN were largely dominated by the $<20 \mu m$ size
249 fraction (63-85 % Fig. 4b) while CIL were mostly represented by the $20-40 \mu m$ and $<20 \mu m$ size
250 fractions (mean 50 and 32%, respectively, Fig. 4d). The biomass of DIN was higher than CIL by
251 factors of 1.3-2.3 at five out of the eight stations. DIN and CIL had, however, equal biomass at M2-2,
252 M1, and M3-3 (Fig. 4 e, f). The DIN+CIL biomass was slightly higher at M2 (mean $3.5 \pm 0.2 \mu g L^{-1}$)
253 than off-plateau ($2.2 \pm 0.3 \mu g L^{-1}$, Fig. 4e). The vertical profiles did not show any noticeable
254 evolution over time at M2 or at the other stations (Fig. 5).

255 A total of 40 morphotypes of DIN and CIL were identified by microscopy at the highest possible
256 taxonomic level. The 23 identified DIN-morphotypes belonged to 13 genera. The genus
257 *Gymnodinium* ($<20\mu m$ in size) was the most abundant DIN and largely prevailed at all stations (Fig.
258 6a). Other small sized DIN such as *Scripsiella*, *Prorocentrum compressum*, and *Amphidinium* were
259 present and abundant at all stations. The larger size classes were represented by *Tripos* and
260 *Dinophysis*, while a variety of *Protoperidinium* morphotypes belonged to small and larger size
261 classes. As for abundance and biomass, DIN richness and community structure were similar at all
262 stations on- and off-plateau (Fig. 6a). The 13 CIL-morphotypes covered 11 genera. *Lohmaniella*
263 *oviformis* ($<20\mu m$ in size) was the most abundant CIL at all stations, with the exception of M3 where
264 the tintinnid *Cymatocylis antarctica* prevailed (Fig. 6b, Table 2). *Leegardiella*, *Codonelopsis soyai*,
265 *Salpingella acuminata*, and *Myrionecta* were present at all stations at low abundances. Finally, the
266 large mixotrophic *Laboea* was relatively abundant during the last two visits at M2, while it was rare
267 at the other stations (Fig. 6b)

268 3.2.2 Molecular diversity vs morphological diversity.

269 Heatmaps illustrating sequencing richness and relative abundance of DIN and CIL are presented in
270 Figure 6c, d. After downstream analysis and elimination of a few symbionts and parasites (e.g.,
271 *Blastodinium* and *Chytriodinium*), the class Dinophyceae was represented by 31 ASVs. (Fig. c).
272 ASVs affiliated to *Tripos* were the most abundant ASVs among those affiliated to DIN (% of reads)
273 in the large size fraction. In the small size fraction, *Tripos* and *Gymnodinium* ASVs were more or less
274 equally represented (Fig. 6c). As in microscopy data, *Gyrodinium* and *Prorocentrum* were also
275 among the most abundant in terms of proportions of reads. However, *Scripsiella* and *Amphidinium*,
276 which were abundant in microscopy, were not found in sequencing data (Fig. 6a, c). A maximum

277 likelihood tree (Fig. 7a) was constructed in order to visualize the relatedness of taxa identified by
278 microscopy and sequencing. Besides sequences generated in this study, additional sequences from
279 the Genbank database corresponding to missing genera observed only by microscopy (e.g.,
280 *Amphidinium* and *Scrippsiella*) were included. The DIN genera *Oxytoxum* and *Katodinium*, which
281 were observed by microscopy, were not represented by sequences in the Genbank or in the PR²
282 (Guillou et al. 2012) databases. They were therefore not included in the tree (Fig. 7a). Most DIN
283 genera in the maximum likelihood tree did not cluster by order, which was especially evident for
284 Gymnodiniales and Peridinales (Fig. 7a). The abundance ranking of taxa differed between
285 sequencing and microscopy (Fig. 6a,c).

286 The ciliate ASVs were grouped into 40 approximate genera with often uncertain taxonomic
287 affiliations below the class or order level (Fig. d). The maximum likelihood tree for CIL included
288 sequences from this study and additional sequences from the Genbank database corresponding to
289 missing genera observed only by microscopy (*Myrionecta*, *Scuticociliatia*, and *Laboea*). The CIL
290 maximum likelihood tree was better resolved than the tree for the DIN with almost all genera
291 clustering by order. The CIL *Codoneopsis* and *Lohmaniella*, *L. oviformis* were the most abundant
292 taxa based on microscopy, but were lacking from the tree since they were not represented by
293 sequences in public databases (Fig. 7b). At M3-1 and M3-3, an ASV affiliated to the tintinnid family
294 Xystonellidae prevailed in the large size fraction (20-100 μm) while *Cymatocylis calyciformis* was
295 the most abundant tintinnid in the microscopy dataset (Fig. 6 c, d). *Myrionecta* is a cosmopolitan CIL
296 characterized by a particular morphology and also several morphotypes grouped into “scuticociliates”
297 were observed by microscopy but were not retrieved by sequencing.

298 3.3 Microzooplankton relation with pigment signatures.

299 COIA analysis was applied to test for spatiotemporal relation in DIN+CIL community composition
300 and phytoplankton pigments (Fig. 8a-e). Hierarchical clustering and PCA of DIN+CIL abundances
301 applied as the first step of the COIA analysis revealed that the on- and off- plateau MOBYDICK
302 stations grouped together (Fig. 8a, c). A3-1, sampled in early spring before the onset of the bloom,
303 grouped with the reference HNLC station (R, sampled during the same cruise), while A3-2 was
304 highly differentiated from all stations in the PCA (Fig. 8a, c). In fact, PCA suggested that station A3-
305 2 was characterized by the presence of the diatom consumers *Gyrodinium* and *Protoperdinium*. In
306 contrast, all MOBYDICK stations were featuring *Gymnodinium*, *Leegardiella*, *Lohmaniella*,
307 *Scrippsiella* and Tintinninds (Fig. 8c). Hierarchical clustering and PCA performed on pigment data
308 indicated similar phytoplankton communities at off-plateau stations during the MOBYDICK cruise.

309 The PCA highlighted a gradual change in pigment signature during the three visits at M2 related to
310 an increase in prasinophyte pigment concentrations. The station A3 was uniquely characterized by
311 high concentrations of diatom pigments and Chl *a* (Fig. 8b, d see also Fig. 3). The COIA
312 multidimensional correlation coefficient (RV) used to estimate the strength of coupling between the
313 pigment concentration and microzooplankton abundance was significant (RV= 0.602, p=0.005) and
314 the first two axes explained 85.65 % of the projected variance (Fig. 8e). All the pigments showed
315 significant correlations (p <0.05, Table A1) with at least one of the three first axes, while ten out of
316 the sixteen genera used for the analysis showed significant correlations : *Gymnodinium*, *Gyrodinium*,
317 *Scrpsiella*, *Amphidinium*, *Tripos*, *Lohmaniella*, *Strombidium*, *Leegaardiella*, *Salpingella*, and
318 *Myrionecta* (Table A1). The COIA scatterplot indicated the station position relative to their DIN, CIL
319 and pigment variables. On the COIA scatterplot MOBYDICK off-plateau stations formed one group
320 with M1 being slightly differentiated potentially due to the influence from the Polar Front. The
321 position of station M1 also changed most between the two PCA-Biplots, as its microzooplankton
322 community strongly resembled the communities at the other off-plateau stations, while its pigment
323 signature was more similar to station M2-2. The first two visits at M2 were close together, while M2-
324 3 was closer to the early spring reference station R, with which it shared a stronger prasinophyte
325 signature. Station A3-2, uniquely representing typical bloom conditions with high diatom pigments
326 and microphytoplankton grazers, was far apart from the other stations in this plot (Fig. 8e).

327

328 3.4 Microzooplankton herbivory via dilution experiments

329 In situ (10-20m depth) Chl *a* concentration measured at the beginning of the dilution experiment
330 varied from 0.20 to 0.64 $\mu\text{g Chl } a \text{ L}^{-1}$ (M3-1 and M2-3, respectively). Dilution derived phytoplankton
331 growth (k) and microzooplankton grazing (g) were significant at all stations (Table 2, Fig. A1).
332 Phytoplankton growth rate (k) ranged from $0.08 \pm 0.03 \text{ d}^{-1}$ at M4-1 to $0.26 \pm 0.03 \text{ d}^{-1}$ at M2-3.
333 Minimum microzooplankton grazing rates (g) were measured at station M1 ($0.28 \pm 0.03 \text{ d}^{-1}$) and the
334 maximum value was at station M2-3 ($0.52 \pm 0.05 \text{ d}^{-1}$). Phytoplankton mortality due to
335 microzooplankton grazing was always higher than phytoplankton growth, representing 130 to 428%
336 of phytoplankton daily production at M1 and M4-1, respectively. Overall, phytoplankton growth rate
337 increased at station M2 (0.13 ± 0.03 to $0.26 \pm 0.03 \text{ d}^{-1}$) along with microzooplankton grazing ($0.34 \pm$
338 0.05 to $0.52 \pm 0.05 \text{ d}^{-1}$, Table 2).

339

340

341

342 4. Discussion

343 The present study showed that ciliates were always recorded at considerably lower abundances than
344 dinoflagellates. The diversity assessed by Illumina sequencing of 18S rDNA amplicons and
345 microscopic observations could be compared with microscopy at a relatively high taxonomic level
346 (i.e., often to family level). In particular for dinoflagellates, relative abundances and ranking of
347 dominant taxa differed between sequencing and microscopy observations. Dilution experiments
348 suggested significant grazing of microzooplankton on phytoplankton as phytoplankton net growth (k)
349 was lower than microzooplankton grazing (g) at all stations. Despite its great potential as
350 phytoplankton grazer, microzooplankton occurred at low biomass and showed little temporal
351 variability, suggesting that it was controlled by copepod predation. These important results are
352 discussed below.

353 4.1 Microzooplankton diversity - microscopy vs sequencing

354 Massive sequencing technologies such as Illumina MiSeq gain *in momentum* (e.g., Pawlowski et al.
355 2012) and are currently used to describe global patterns of plankton and even predict carbon export
356 (e.g., Guidi et al. 2016, Obiol et al. 2020, among many others). The recent ASV approach is supposed
357 to provide a more accurate image of the diversity by avoiding artificial similarity thresholds.
358 Nevertheless, organisms differing by a few base pairs in their rDNA can belong to very different taxa
359 and the threshold of differences in the rDNA sequence between species differs greatly from one
360 taxonomic group to another one because of their evolution rate for example. Defining accurate
361 taxonomy level based on the sequencing of rDNA remains a critical issue in microbial diversity
362 investigations. In-depth sequencing and microscopy approaches are rarely confronted although they
363 both 'miss' or 'misidentify' taxa due to the diverse biases inherent to each method (e.g., Medinger et al.
364 2010; Bachy et al. 2012; Chavret et al. 2012; Stern et al. 2018 and references therein). We address
365 this by combining high throughput sequencing with microscopic observations to assess DIN and CIL
366 diversity. Although microscopy and sequencing heatmaps (Fig. 6a-d) cannot be directly compared
367 (different size fractions and water volumes analyzed for the two approaches), the diversity and
368 abundance data obtained by the two approaches can be assessed to determine whether these results
369 are conflicting or complementary. DIN were represented by 23 morphospecies in microscopy and 31
370 ASVs in sequencing data. Microscopic identification of dinoflagellates based on broad
371 morphological features is challenging. On the other hand, amplicon sequencing does not provide
372 accurate taxonomic resolution because of the lack of cultured representatives to provide a detailed
373 phylogeny. This is the case for dinoflagellate taxa that are under-represented in databases, resulting

374 in approximate taxonomic identifications of sequences and diversity estimates (e.g., Bik et al. 2012).
375 Most DIN genera did not cluster by order in the topologic tree, which was especially evident for
376 Gymnodiniales and Peridinales (Fig. 7a). This insufficient resolution of DIN phylogeny might be
377 due to the limited length and low variability of the V3-V4 region in the 18S rDNA (Daugbjerg et al.
378 2000; Mordret et al. 2018). A relatively good ‘correspondence’ was found between the two data sets
379 in terms of diversity, but often at a higher taxonomic level, either at the family or order level (Fig. 6a,
380 c). For example, the second most abundant genus found in microscopy identified as *Scrippsiella* was
381 probably represented by the family level Thoracosphaeracea in sequencing data (Fig. 6a, c). However,
382 no potential ‘relative’ for *Amphidinium* could be found in sequencing data (Fig. 7a). Sequencing
383 complemented microscopy data in terms of diversity. Because the sample volume analyzed for
384 microscopy counts is relatively limited, in contrast to the sequencing approach, low abundant taxa
385 may not be observed by microscopy despite their characteristic morphological features. This was
386 likely the case for the genus *Ornithocercus* (ASV 508) that was also retrieved in the vertically
387 integrated plankton-net samples, where very large volumes of water were sampled (Karine Leblanc,
388 <https://plankton.mio.osupytheas.fr/mobydick-other-microplankton/>). In addition, taxa relative
389 abundance differed among sequencing and microscopy. It is well established that DIN are over-
390 represented in sequencing data (e.g., Georges et al. 2014 and references therein). The dominance of
391 *Triplos* in sequencing data - even in the small fraction - (Fig. 6c) highlighted that, even within the
392 DIN population, specific taxa can be over-represented. As a consequence, using relative abundances
393 of DIN based on sequence data in numerical analysis and/or description of community structure
394 might lead to biases.

395 CIL were represented by 17 morphospecies in microscopy and 40 genera in sequencing data. The
396 difficulty to accurately identify CIL based on broad morphology is exacerbated by the distortion of
397 soft CIL due to chemical fixation. Only tintinnids having a lorica, preserve most of their features (e.g.,
398 Dolan et al. 2012). As for DIN, comparison of sequencing and microscopy data was challenging, in
399 particular at the genus level, but could be attempted at higher taxonomic levels. Although, the CIL
400 maximum likelihood tree had a better resolution than the topology of DIN, CIL sequencing and
401 microscopy data could only be globally compared at a higher level than the DIN data (i.e., family,
402 order, or class level). For example, *Lohmanniella oviformis*, which was the most abundant species in
403 microscopy, was probably represented by *Leegardiella* in sequencing data (family Leegaardiellidae,
404 Lynn and Montagnes, 1988). *Strombidium* was the second most abundant genus in both data sets. At
405 M3-1 and M3-3, the family Xystonellidae, order Tintinnida prevailed in the large size fraction (20-
406 100 μm) according to sequencing data. At the same stations, the dominant tintinnid in microscopy

407 data was identified as *Cymatocylis calyciformis* that belongs to a different family (Ptychocyliidae)
408 but to the same order (Tintinnida) (Fig. 6 b, d). The organisms grouped into ‘scuticociliates’ in
409 microscopy data probably belonged to different families or classes. Within the CIL populations, there
410 was no evidence of over-representation of specific taxa and the ranking of the different taxonomic
411 groups obtained by sequencing corresponded more or less to the one by microscopy. The taxonomic
412 resolution obtained by sequencing was lower than the one obtained by microscopy (Fig. 6b, d).

413 As a conclusion, applying both sequencing and microscopy analyses to DIN and CIL can
414 complement and enrich our view on the population diversity. However, if available, microscopy
415 based abundances seem more reliable for numeric analysis. Using DIN relative abundances (retrieved
416 from sequencing data) for numerical analysis could lead to misinterpretations of the importance of
417 different taxa for ecosystem functioning. Therefore, morphological metadata can and should be
418 collected in parallel to sequencing of DIN and CIL.

419 4.2 The relation of late summer microzooplankton communities to phytoplankton

420 Microzooplankton community structure and the biomass quantity are expected to relate to shifts in
421 phytoplankton community composition (e.g., Grattepanche et al. 2011a; Laurence and Menden-
422 Deuer 2012). Although other components of the microbial food web showed > 2-3 fold higher
423 abundance and activity on the plateau, and remained highly dynamic during the MOBYDICK cruise
424 (Christaki et al. 2021; e.g., 2-fold increase in Chl *a* concentrations to 0.58 $\mu\text{g L}^{-1}$ during the third visit
425 to M2, Table 1), the DIN and CIL biomass was only ~ 1.5 x higher on-plateau (M2) compared to off-
426 plateau and showed little temporal variability (e.g., Fig. 4). As a result, stations clustered differently
427 based on pigment or microzooplankton data (Fig. 8a-d). The variability of the abundance of
428 prasinophytes at M2, A3-1, R and the diatom increase at A3-2, were highlighted by the same analysis
429 (Figs. 8c, d). The rapid increase in prasinophytes and diatoms on the plateau (M2 during
430 MOBYDICK) was likely driven by changes in environmental conditions, such as NH_4 concentrations
431 (Irion et al. 2020, Sassenhagen et al. 2020), which the microzooplankton community did not follow
432 in the observed time frame. However, considering all data, the COIA analysis showed that there was
433 an overall significant relationship between microzooplankton abundances and pigment concentrations
434 ($p=0.005$, Fig. 8e).

435 The maximum abundance of dinoflagellates and ciliates was often observed at the base of the ML
436 (Table 1, Fig. 5, Christaki et al. 2008, 2015) and coincided with the formation of the deep chlorophyll
437 maximum (DCM) (Lasbleiz *et al.* 2014). The formation of a DCM is described as a recurrent feature

438 in the Southern Ocean, and is explained by the accumulation of inactive, though living, algal cells,
439 mainly composed of diatoms (Uitz *et al.* 2009 and references therein).

440 The correlation between DIN biomass and phytoplankton abundance was especially noticeable
441 during the onset of the diatom bloom on the plateau (Lasbleiz *et al.* 2016, Figs. 3 and 8, KEOPS2).
442 The abundance and biomass of DIN increased 8 and 7 fold, respectively, within 3.5 weeks between
443 the visits at station A3. In particular, large dinoflagellates such as *Gyrodinium* (40-60 μm),
444 *Amphidinium* (20-40 μm) and *Protoberidinium*, which feed on diatoms and can ingest prey cells of
445 more than 10 x their own size (e.g., Saito *et al.* 2006, Grattepanche *et al.* 2011b), occurred in higher
446 abundance after the intensification of the bloom (Figs. 6a, 8, Christaki *et al.* 2015).

447 During MOBYDICK, a common feature of DIN and CIL communities was the relative importance of
448 small cells (<40 μm) which was particularly pronounced for DIN (Fig. 4b). Small sized *Gymnodinium*
449 were the most abundant DIN taxa at all stations and during both seasons (<20 μm , see also Christaki
450 *et al.* 2015). *Gymnodinium* can grow in a wide range of environmental conditions due to two
451 particular traits. Their mixotrophy allows them to switch between photosynthesis and grazing
452 depending on present nutrient, prey and light conditions, while they can also feed on a wide range of
453 prey (including other DIN, CIL, and bacteria) (e.g., Strom, 1991; Bockstalher and Coats, 1993; Sherr
454 and Sherr, 2007; Sherr and Sherr, 2007; Jeong *et al.* 2010, 2018; Lee *et al.* 2014).

455 CIL abundances were considerably lower than those of DIN, the median for all stations and seasons
456 being 350 and 1370 cells L^{-1} , respectively (Figs. 4a, c, Fig. 5). DIN can graze on almost all
457 planktonic organisms and are recognized as major microplankton predators (Sherr and Sherr, 2007).
458 In contrast, naked CIL prefer prey of the 5-25 μm size-class (Hansen *et al.* 1994) and can also feed
459 on bacteria (Sherr and Sherr, 1987; Christaki *et al.* 1998; 1999). The most abundant CIL during
460 MOBYDICK was *Lohmaniella oviformis* belonging to the <20 μm size class. CIL abundance and
461 biomass were higher after the bloom than during the onset of the bloom. This pattern was likely
462 related to the increase in abundance of their nanophytoplankton preys. However, while pico- and
463 nanophytoplankton increased by about 15-fold between the onset and the post bloom periods in
464 Kerguelen plateau waters (Christaki *et al.* 2014; Irion *et al.* 2020), CIL abundance increased only by
465 about 1.4 and 2.5 on- and off-plateau, respectively (Fig. 4c). Also, during MOBYDICK, pico- and
466 nanoplankton showed a 2.6-fold increase between the first and the third visit at M2 (Irion *et al.* 2020),
467 while CIL slightly decreased (Fig. 4c). The overall CIL abundance was always relatively low and
468 never exceeded 450 cells L^{-1} . The absence of any clear relation between the abundance of CIL and
469 their favorite prey was likely the result of the double top-down control on ciliates by both
470 dinoflagellates and mesozooplankton (Calbet and Saiz, 2005; Franzé and Modigh, 2013). CIL have
471 not been shown to effectively feed on large or chain-forming diatoms (Sherr and Sherr, 2007). Only

472 tintinnid CIL can feed on a large variety of small diatoms (Gowing and Garrison, 1992; Armbréghet et
473 al. 2017). The tintinnids located in the Antarctic zone, delimited by the average location of the Polar
474 Front, contain a large portion of wide-mouthed forms (Dolan et al. 2012). The ability of relatively
475 large tintinnids, in 40-60 μm and 60-100 μm size-classes, to ingest small diatoms is probably an
476 advantage that allows them to form dense populations in SO (e.g., Alder and Boltovskoy 1991; Buck
477 et al. 1992; Dolan et al. 2012). Indeed, *Cymatocylis antarctica* was the second most abundant CIL
478 and was particularly present at the HNLC M3-station where small diatoms ($<20 \mu\text{m}$) were also
479 enhanced (*Fragilariopsis*, *Pseudo-nitzschia*, *Thalassiosira* and *Chaetoceros*, Irion et al. 2020).

480 4.3 Potential role of microzooplankton in carbon transfer in planktonic food webs

481 Comprehensive assessment of grazing in natural phytoplankton communities is still very challenging
482 and relies on many assumptions. One widely used approach is the relatively simple dilution method
483 which estimates grazing rates based on phytoplankton growth in a gradient of grazing pressure.
484 Among the criticisms of the dilution method are that dilution experiments may provide inconsistent
485 results, i.e., abnormally high and/or null grazing rates (e.g., Dolan and McKeon 2005, Calbet et al.
486 2011; Calbet and Saiz 2013). The dilution experiment estimated grazing by the whole heterotrophic
487 community $< 200 \mu\text{m}$, including heterotrophic nanoflagellates. During MOBYDICK, heterotrophic
488 nanoflagellates and their grazing on picoplankton were quantified. The nanoflagellates grazed almost
489 exclusively on heterotrophic bacteria (Christaki et al. 2021). Thus, the high grazing rates measured in
490 the dilution experiments were most likely dominated by microzooplankton grazing. This is in line
491 with the finding that the small sized phytoplankton community was dominated by nano-sized
492 Prymnesiophytes (Irion et al. 2020); and that small phytoplankton cells, which are the preferred
493 microzooplankton prey (prymnesiophytes, prasinophytes and small diatoms), were actively growing
494 ($0.22\text{-}0.37 \text{ division d}^{-1}$, Irion et al. 2021).

495 One potential caveat with the dilution experiment is that photoacclimation of phytoplankton to stable
496 light conditions in the incubator may have resulted in reduced Chl *a* concentrations compared to T0
497 and underestimation of growth rates, (Ross et al. 2011).

498 Another potential caveat with the dilution experiment is reduced phytoplankton growth due to
499 nutrient limitation over the course of the experiment. However, measurements of macro-nutrient
500 concentrations at all stations during the cruise did not suggest any limitations and the noticeable
501 increase in phytoplankton biomass at M2 indicated sufficient iron concentrations even in late summer
502 after the decline of the bloom. Depletion of nutrients to limiting levels over the short duration of the
503 experiments (24h) was therefore unlikely. The phytoplankton growth rate (μ) and the
504 microzooplankton grazing rate (g) measured during MOBYDICK in the dilution experiments were

505 within the range of previous studies in cold waters (e.g., Menden-Deuer et al. 2018; Schmoker et al.
506 2013 and references therein). Phytoplankton growth was lower than microzooplankton grazing at all
507 stations (Table 2). Our data add to the surprisingly high variability of estimates of standing stock of
508 phytoplankton grazed by microzooplankton in the Southern Ocean, (from 0 to >100 %, median \approx
509 50 %, Schmoker et al. 2013).

510

511 Given the limitations and assumptions of the dilution method, these estimates of phytoplankton
512 consumption by microzooplankton were compared with the CD (Carbon Demand) of DIN and CIL as
513 a proportion of GCP (Gross Community Production) and NCP (Net Community Production). The
514 CD was calculated based on their biomass stocks applying a conservative growth rate $\mu = 0.2 \text{ d}^{-1}$ (e.g.,
515 Bjørnsen and Kuparinen, 1991; Verity et al. 1993; Neuer and Cowles, 1994; Karayanni et al. 2008;
516 Rose et al. 2013) and a growth efficiency (GE) of 30% (e.g., Straile, 1997; Strom, 1991; Strom and
517 Fredrickson, 2008). According to these estimates, the carbon demand of DIN and CIL accounted for
518 5 and 3 % of the GCP on- and off-plateau, respectively, in late summer. It was, however,
519 considerably higher on the plateau during the onset of the bloom where it accounted for 18 % of the
520 GCP (station A3-2, Table 3). The proportion of carbon corresponding to CD changed when NCP
521 (Net Community Production) was taken into account due to the variability in DCR (Dark Community
522 Respiration) among stations. Thus, the amount of NCP needed to cover the DIN+CIL carbon demand
523 varied between 5-46 % (Table 3). To note, that these estimations of CD and NCP should be
524 considered as conservative since they were based on stocks and literature conversion factors.

525

526 The low abundance of microzooplankton despite high grazing rates could also be explained by intra-
527 guild predation which is common for these mixotrophic and heterotrophic organisms (e.g., Franzé
528 and Modigh 2013) and strong top-down-control through mesozooplankton such as copepods.

529 In particular, after the end of the bloom (MOBYDICK), the low nutritional quality of phytoplankton
530 probably further enhanced top-down control on microzooplankton by copepods (Sherr et al. 2009;
531 Tsuda et al. 2007). During MOBYDICK, two observations lend support for mesozooplankton top-
532 down control on microzooplankton. First, mesozooplankton abundance showed large variability,
533 ranging between 207 ind. m^{-3} at M2-1 to 1636 ind. m^{-3} at M4-1, and in particular at M2 where it
534 showed a 7-fold increase between the first and the second visit (1473 ind. m^{-3}) at this station.
535 Secondly, grazing experiments showed that there was insignificant grazing of copepods on
536 phytoplankton and that their respiration requirements were never covered by phytoplankton ingestion

537 (Delegrange et al. MOBYDICK unpublished data) suggesting that they were primarily grazing on
538 microzooplankton.

539

540 In conclusion, the present study provides two interesting observations: (i) dilution experiments
541 indicated high microzooplankton grazing capacity on phytoplankton; and (ii) microzooplankton
542 biomass remained low, suggesting a top-down feeding impact by copepods. We suggest that DIN and
543 CIL activities, and thus their roles in the trophic web of surface SO waters, are highly dynamic,
544 however, this is not necessarily reflected in their stock variability. Microzooplankton can apparently
545 not prevent phytoplankton bloom initiations (Sherr and Sherr, 2009), likely due to substantial
546 zooplankton predation on microzooplankton (Stoecker and Capuzzo, 1990). Our observations
547 highlighted the decoupling between microzooplankton stocks (abundance and biomass) and activities
548 (C-transfer) in SO surface waters. Estimations of carbon transfer solely based on microzooplankton
549 stocks will thus likely lead to incorrect results. The strength of the microzooplankton-
550 mesozooplankton relationship is rarely considered in plankton studies (e.g., Foreman et al. 1996;
551 Calbet and Saiz, 2005) and typically neglected in the construction of carbon budgets. The question is
552 therefore: How do we parametrize microzooplankton in ecosystem models? Strom and Fredrickson
553 (2008) recommended to parametrize microzooplankton grazing as a ‘sometimes-on, frequently-off’
554 response, rather than a low average. Microzooplankton biomass increases typically during brief
555 periods of time before copepod populations establish, as seen during the onset of the bloom when
556 high DIN biomass was correlated with large diatom grazers on the plateau (Fig. 4, second visit at A3,
557 Christaki et al. 2015). We suggest, that outside this period, when microzooplankton biomass remains
558 low, it continues to play a crucial role as they ‘repackage’ and ‘enrich’ phytoplankton carbon for
559 higher trophic levels, and also contribute to nutrient and Fe regeneration (Sarhou et al. 2008).

560

561 Acknowledgements We thank B. Quéguiner, the PI of the MOBYDICK project, for providing us the
562 opportunity to participate to this cruise, the captain and crew of the R/V Marion Dufresne for their
563 enthusiasm and support aboard during the MOBYDICK–THEMISTO cruise
564 (<https://doi.org/10.17600/18000403>) and the chief scientist I. Obernosterer. This work was supported
565 by the French oceanographic fleet (“Flotte océanographique française”), the French ANR (“Agence
566 Nationale de la Recherche”, AAPG 2017 program, MOBYDICK Project number: ANR-17-CE01-
567 0013), and the French Research program of INSU-CNRS LEFE/CYBER (“Les enveloppes fluides et
568 l’environnement” – “Cycles biogéochimiques, environnement et ressources”). This work was also
569 supported by ULCO (Université du Littoral), CPER MARCO (<https://marco.univ-littoral.fr/>), the

570 Region "Hauts de France" and CNRS LEFE-EC2CO through the project PLANKTON-PARTY. The
571 authors clearly state there is no conflict of interests regarding this paper.

572

573 References

574 Alder, V.A., Boltovskoy, D., 1991. Microplanktonic distributional patterns west of the Antarctic
575 Peninsula, with special emphasis on the Tintinnids. *Polar Biol* 11, 103–112.
576 <https://doi.org/10.1007/BF00234272>

577 Armand, L.K., Cornet-Barthaux, V., Mosseri, J., Quéguiner, B., 2008. Late summer diatom biomass
578 and community structure on and around the naturally iron-fertilised Kerguelen Plateau in the
579 Southern Ocean. *Deep Sea Research Part II: Topical Studies in Oceanography* 55, 653–676.
580 <https://doi.org/10.1016/j.dsr2.2007.12.031>

581 Armbrecht, L.H., Eriksen, R., Leventer, A., Armand, L.K., 2017. First observations of living sea-ice
582 diatom agglomeration to tintinnid loricae in East Antarctica. *Journal of Plankton Research* 39,
583 795–802. <https://doi.org/10.1093/plankt/fbx036>

584 Bachy, C., Dolan, J.R., López-García, P., Deschamps, P., Moreira, D., 2013. Accuracy of protist
585 diversity assessments: morphology compared with cloning and direct pyrosequencing of 18S
586 rRNA genes and ITS regions using the conspicuous tintinnid ciliates as a case study. *The*
587 *ISME Journal* 7, 244–255. <https://doi.org/10.1038/ismej.2012.106>

588 Beckett, S.J., Weitz, J.S., 2017. Disentangling niche competition from grazing mortality in
589 phytoplankton dilution experiments. *PLoS ONE* 12, e0177517.
590 <https://doi.org/10.1371/journal.pone.0177517>

591 Bik, H.M., Porazinska, D.L., Creer, S., Caporaso, J.G., Knight, R., Thomas, W.K., 2012. Sequencing
592 our way towards understanding global eukaryotic biodiversity. *Trends in Ecology &*
593 *Evolution* 27, 233–243. <https://doi.org/10.1016/j.tree.2011.11.010>

594 Bjørnson, P.K., Kuparinen, J., 1991. Growth and herbivory by heterotrophic dinoflagellates in the
595 Southern Ocean, studied by microcosm experiments. *Mar. Biol.* 109, 397–405.
596 <https://doi.org/10.1007/BF01313505>

597 Blain, S., Quéguiner, B., Armand, L., Belviso, S., Bombled, B., Bopp, L., Bowie, A., Brunet, C.,
598 Brussaard, C., Carlotti, F., Christaki, U., Corbière, A., Durand, I., Ebersbach, F., Fuda, J.-L.,
599 Garcia, N., Gerringa, L., Griffiths, B., Guigue, C., Guillerm, C., Jacquet, S., Jeandel, C.,
600 Laan, P., Lefèvre, D., Lo Monaco, C., Malits, A., Mosseri, J., Obernosterer, I., Park, Y.-H.,
601 Picheral, M., Pondaven, P., Remenyi, T., Sandroni, V., Sarthou, G., Savoye, N., Scouarnec,

602 L., Souhaut, M., Thuiller, D., Timmermans, K., Trull, T., Uitz, J., van Beek, P., Veldhuis, M.,
603 Vincent, D., Viollier, E., Vong, L., Wagener, T., 2007. Effect of natural iron fertilization on
604 carbon sequestration in the Southern Ocean. *Nature* 446, 1070–1074.
605 <https://doi.org/10.1038/nature05700>

606 Blain, S., Capparos, J., Guéneuguès, A., Obernosterer, I., Oriol, L., 2015. Distributions and
607 stoichiometry of dissolved nitrogen and phosphorus in the iron-fertilized region near
608 Kerguelen (Southern Ocean). *Biogeosciences* 12, 623–635. <https://doi.org/10.5194/bg-12-623-2015>

610 Bockstahler, K.R., Coats, D.W., 1993. Grazing of the mixotrophic dinoflagellate *Gymnodinium*
611 *sanguineum* on ciliate populations of Chesapeake Bay. *Marine Biology* 116, 477–487.
612 <https://doi.org/10.1007/BF00350065>

613 Bower, S.M., Carnegie, R.B., Goh, B., Jones, S.R.M., Lowe, G.J., Mak, M.W.S., 2004. Preferential
614 PCR Amplification of Parasitic Protistan Small Subunit rDNA from Metazoan Tissues. *J*
615 *Eukaryotic Microbiology* 51, 325–332. <https://doi.org/10.1111/j.1550-7408.2004.tb00574.x>

616 Brussaard, C.P.D., Timmermans, K.R., Uitz, J., Veldhuis, M.J.W., 2008. Virioplankton dynamics and
617 virally induced phytoplankton lysis versus microzooplankton grazing southeast of the
618 Kerguelen (Southern Ocean). *Deep Sea Res. II*, 44, 752-765. doi:10.1016/j.dsr2.2007.12.034

619 Buck, K.R., Garrison, D.L., Hopkins, T.L., 1992. Abundance and distribution of tintinnid ciliates in
620 an ice edge zone during the austral autumn. *Antartic science* 4, 3–8.
621 <https://doi.org/10.1017/S0954102092000038>

622 Calbet, A., Landry, M.R., 2004. Phytoplankton growth, microzooplankton grazing, and carbon
623 cycling in marine systems. *Limnol. Oceanogr.* 49, 51–57.
624 <https://doi.org/10.4319/lo.2004.49.1.0051>

625 Calbet, A., Saiz, E., 2005. The ciliate-copepod link in marine ecosystems. *Aquat. Microb. Ecol.* 38,
626 157–167. <https://doi.org/10.3354/ame038157>

627 Calbet, A., Saiz, E., Almeda, R., Movilla, J.I., Alcaraz, M., 2011. Low microzooplankton grazing
628 rates in the Arctic Ocean during a *Phaeocystis pouchetii* bloom (Summer 2007): fact or
629 artifact of the dilution technique? *Journal of Plankton Research* 33, 687–701.
630 <https://doi.org/10.1093/plankt/fbq142>

631 Calbet, A., Saiz, E., 2013. Effects of trophic cascades in dilution grazing experiments: from artificial
632 saturated feeding responses to positive slopes. *Journal of Plankton Research* 35, 1183–1191.
633 <https://doi.org/10.1093/plankt/fbt067>

634 Callahan, B.J., McMurdie, P.J., Rosen, M.J., Han, A.W., Johnson, A.J.A., Holmes, S.P., 2016.
635 DADA2: High-resolution sample inference from Illumina amplicon data. *Nat Methods* 13,

636 581–583. <https://doi.org/10.1038/nmeth.3869>

637 Campbell, R.G., Sherr, E.B., Ashjian, C.J., Plourde, S., Sherr, B.F., Hill, V., Stockwell, D.A., 2009.

638 Mesozooplankton prey preference and grazing impact in the western Arctic Ocean. *Deep Sea*

639 *Research Part II: Topical Studies in Oceanography* 56, 1274–1289.

640 <https://doi.org/10.1016/j.dsr2.2008.10.027>

641 Capella-Gutierrez, S., Silla-Martinez, J.M., Gabaldon, T., 2009. trimAl: a tool for automated

642 alignment trimming in large-scale phylogenetic analyses. *Bioinformatics* 25, 1972–1973.

643 <https://doi.org/10.1093/bioinformatics/btp348>

644 Caporaso, J.G., Kuczynski, J., Stombaugh, J., Bittinger, K., Bushman, F.D., Costello, E.K., Fierer,

645 N., Peña, A.G., Goodrich, J.K., Gordon, J.I., Huttley, G.A., Kelley, S.T., Knights, D., Koenig,

646 J.E., Ley, R.E., Lozupone, C.A., McDonald, D., Muegge, B.D., Pirrung, M., Reeder, J.,

647 Sevinsky, J.R., Turnbaugh, P.J., Walters, W.A., Widmann, J., Yatsunenko, T., Zaneveld, J.,

648 Knight, R., 2010. QIIME allows analysis of high-throughput community sequencing data. *Nat*

649 *Methods* 7, 335–336. <https://doi.org/10.1038/nmeth.f.303>

650 Caron, D.A., Dennett, M.R., Lonsdale, D.J., Moran, D.M., Shalapyonok, L., 2000. Microzooplankton

651 herbivory in the Ross Sea, Antarctica. *Deep Sea Research Part II: Topical Studies in*

652 *Oceanography* 47, 3249–3272. [https://doi.org/10.1016/S0967-0645\(00\)00067-9](https://doi.org/10.1016/S0967-0645(00)00067-9)

653 Caron, D.A., Worden, A.Z., Countway, P.D., Demir, E., Heidelberg, K.B., 2009. Protists are

654 microbes too: a perspective. *ISME J* 3, 4–12. <https://doi.org/10.1038/ismej.2008.101>

655 Caron, D.A., Countway, P.D., Jones, A.C., Kim, D.Y., Schnetzer, A., 2012. Marine Protistan

656 Diversity. *Annu. Rev. Mar. Sci.* 4, 467–493. [https://doi.org/10.1146/annurev-marine-120709-](https://doi.org/10.1146/annurev-marine-120709-142802)

657 142802

658 Caron, D.A., Hutchins, D.A., 2013. The effects of changing climate on microzooplankton grazing

659 and community structure: drivers, predictions and knowledge gaps. *Journal of Plankton*

660 *Research* 35, 235–252. <https://doi.org/10.1093/plankt/fbs091>

661 Cavagna, A.J., Fripiat, F., Elskens, M., Dehairs, F., Mangion, P., Chirurgien, L., Closset, I., Lasbleiz,

662 M., Flores–Leiva, L., Cardinal, D., Leblanc, K., Fernandez, C., Lefèvre, D., Oriol, L., Blain,

663 S., Quéguiner, B., 2014. Biological productivity regime and associated N cycling in the

664 vicinity of Kerguelen Island area, Southern Ocean. *Biogeosciences Discuss.* 11, 18073–

665 18104. <https://doi.org/10.5194/bgd-11-18073-2014>

666 Cavagna, A.J., Fripiat, F., Elskens, M., Mangion, P., Chirurgien, L., Closset, I., Lasbleiz, M., Florez-

667 Leiva, L., Cardinal, D., Leblanc, K., Fernandez, C., Lefèvre, D., Oriol, L., Blain, S.,

668 Quéguiner, B., Dehairs, F., 2015. Production regime and associated N cycling in the vicinity

669 of Kerguelen Island, Southern Ocean. *Biogeosciences* 12, 6515–6528.

670 <https://doi.org/10.5194/bg-12-6515-2015>

671 Charvet, S., Vincent, W.F., Lovejoy, C., 2012. Chrysophytes and other protists in High Arctic lakes:
672 molecular gene surveys, pigment signatures and microscopy. *Polar Biol* 35, 733–748.
673 <https://doi.org/10.1007/s00300-011-1118-7>

674 Chen, B., Landry, M.R., Huang, B., Liu, H., 2012. Does warming enhance the effect of
675 microzooplankton grazing on marine phytoplankton in the ocean? *Limnol. Oceanogr.* 57,
676 519–526. <https://doi.org/10.4319/lo.2012.57.2.0519>

677 Christaki, U., Dolan, J.R., Pelegri, S., Rassoulzadegan, F., 1998. Consumption of picoplankton-size
678 particles by marine ciliates: Effects of physiological state of the ciliate and particle quality.
679 *Limnology and Oceanography* 43, 458–464. <https://doi.org/10.4319/lo.1998.43.3.0458>

680 Christaki, U., Jacquet, S., Dolan, J.R., Vaulot, D., Rassoulzadegan, F., 1999. Growth and grazing on
681 *Prochlorococcus* and *Synechococcus* by two marine ciliates. *Limnol. Oceanogr.* 44, 52–61.
682 <https://doi.org/10.4319/lo.1999.44.1.0052>

683 Christaki, U., Obernosterer, I., Van Wambeke, F., Veldhuis, M., Garcia, N., Catala, P., 2008.
684 Microbial food web structure in a naturally iron-fertilized area in the Southern Ocean
685 (Kerguelen Plateau). *Deep Sea Research Part II: Topical Studies in Oceanography* 55, 706–
686 719. <https://doi.org/10.1016/j.dsr2.2007.12.009>

687 Christaki, U., Lefèvre, D., Georges, C., Colombet, J., Catala, P., Courties, C., Sime-Ngando, T.,
688 Blain, S., Obernosterer, I., 2014. Microbial food web dynamics during spring phytoplankton
689 blooms in the naturally iron-fertilized Kerguelen area (Southern Ocean). *Biogeosciences* 11,
690 6739–6753. <https://doi.org/10.5194/bg-11-6739-2014>

691 Christaki, U., Georges, C., Genitsaris, S., Monchy, S., 2015. Microzooplankton community
692 associated with phytoplankton blooms in the naturally iron-fertilized Kerguelen area
693 (Southern Ocean). *FEMS Microbiology Ecology* 91. <https://doi.org/10.1093/femsec/fiv068>

694 Christaki, U., Guenegues, A., Liu, Y., Blain, S., Catala C., Colombet, J., Debeljak, P., Jardillier, L.,
695 Irion, S., Planchon, F., Sassenhagen, I., Sime-Ngando, T., Ingrid Obernosterer I., 2021.
696 Seasonal microbial food web dynamics in contrasting Southern Ocean productivity regimes.
697 *Limnol Oceanogr* Ino.11591. <https://doi.org/10.1002/lno.11591>

698 Closset, I., Lasbleiz, M., Leblanc, K., Quéguiner, B., Cavagna, A.-J., Elskens, M., Navez, J., Cardinal,
699 D., 2014. Seasonal evolution of net and regenerated silica production around a natural Fe-
700 fertilized area in the Southern Ocean estimated with Si isotopic approaches. *Biogeosciences*
701 11, 5827–5846. <https://doi.org/10.5194/bg-11-5827-2014>

702 Daugbjerg, N., Hansen, G., Larsen, J., Moestrup, Ø., 2000. Phylogeny of some of the major genera of
703 dinoflagellates based on ultrastructure and partial LSU rDNA sequence data, including the

704 erection of three new genera of unarmoured dinoflagellates. *Phycologia* 39, 302–317.
705 <https://doi.org/10.2216/i0031-8884-39-4-302.1>

706 Dolan, J.R., McKeon, K., 2005. The reliability of grazing rate estimates from dilution experiments:
707 Have we over-estimated rates of organic carbon consumption by microzooplankton? *Ocean*
708 *Sci.* 1, 1–7. <https://doi.org/10.5194/os-1-1-2005>

709 Dolan, J.R., Pierce, R.W., Yang, E.J., Kim, S.Y., 2012. Southern Ocean Biogeography of Tintinnid
710 Ciliates of the Marine Plankton. *J. Eukaryot. Microbiol.* 59, 511–519.
711 <https://doi.org/10.1111/j.1550-7408.2012.00646.x>

712 Doledec, S., Chessel, D., 1994. Co-inertia analysis: an alternative method for studying species-
713 environment relationships. *Freshwater Biol* 31, 277–294. <https://doi.org/10.1111/j.1365-2427.1994.tb01741.x>

715 Dray, S., Chessel, D., Thioulouse, J., 2003. CO-INERTIA ANALYSIS AND THE LINKING OF
716 ECOLOGICAL DATA TABLES. *Ecology* 84, 3078–3089. <https://doi.org/10.1890/03-0178>

717 Dray, S., Dufour, A.-B., 2007. The **ade4** Package: Implementing the Duality Diagram for Ecologists.
718 *J. Stat. Soft.* 22. <https://doi.org/10.18637/jss.v022.i04>

719 Edgar, R.C., 2004. MUSCLE: multiple sequence alignment with high accuracy and high throughput.
720 *Nucleic Acids Research* 32, 1792–1797. <https://doi.org/10.1093/nar/gkh340>

721 Franzé, G., Modigh, M., 2013. Experimental evidence for internal predation in microzooplankton
722 communities. *Mar Biol* 160, 3103–3112. <https://doi.org/10.1007/s00227-013-2298-1>

723 Froneman, P., Pakhomov, E., Perissinotto, R., McQuaid, C., 1996. Role of microplankton in the diet
724 and daily ration of Antarctic zooplankton species during austral summer. *Mar. Ecol. Prog.*
725 *Ser.* 143, 15–23. <https://doi.org/10.3354/meps143015>

726 Georges, C., Monchy, S., Genitsaris, S., Christaki, U., 2014. Protist community composition during
727 early phytoplankton blooms in the naturally iron-fertilized Kerguelen area (Southern Ocean).
728 *Biogeosciences* 11, 5847–5863. <https://doi.org/10.5194/bg-11-5847-2014>

729 Gowing, M.M., Garrison, D.L., 1992. Abundance and feeding ecology of larger protozooplankton in
730 the ice edge zone of the Weddell and Scotia Seas during the austral winter. *Deep Sea*
731 *Research Part A. Oceanographic Research Papers* 39, 893–919. [https://doi.org/10.1016/0198-0149\(92\)90128-G](https://doi.org/10.1016/0198-0149(92)90128-G)

733 Grattepanche, J.-D., Breton, E., Brylinski, J.-M., Lecuyer, E., Christaki, U., 2011a. Succession of
734 primary producers and micrograzers in a coastal ecosystem dominated by *Phaeocystis globosa*
735 blooms. *Journal of Plankton Research* 33, 37–50. <https://doi.org/10.1093/plankt/fbq097>

736 Grattepanche, J.-D., Vincent, D., Breton, E., Christaki, U., 2011b. Microzooplankton herbivory
737 during the diatom–*Phaeocystis* spring succession in the eastern English Channel. *Journal of*

738 Experimental Marine Biology and Ecology 404, 87–97.
739 <https://doi.org/10.1016/j.jembe.2011.04.004>

740 Guidi, L., Chaffron, S., Bittner, L., Eveillard, D., Larhlimi, A., Roux, S., Darzi, Y., Audic, S.,
741 Berline, L., Brum, J.R., Coelho, L.P., Espinoza, J.C.I., Malviya, S., Sunagawa, S., Dimier, C.,
742 Kandels-Lewis, S., Picheral, M., Poulain, J., Searson, S., Stemmann, L., Not, F., Hingamp, P.,
743 Speich, S., Follows, M., Karp-Boss, L., Boss, E., Ogata, H., Pesant, S., Weissenbach, J.,
744 Wincker, P., Acinas, S.G., Bork, P., de Vargas, C., Iudicone, D., Sullivan, M.B., Raes, J.,
745 Karsenti, E., Bowler, C., Gorsky, G., 2016. Plankton networks driving carbon export in the
746 oligotrophic ocean. *Nature* 532, 465–470. <https://doi.org/10.1038/nature16942>

747 Guillou, L., Bachar, D., Audic, S., Bass, D., Berney, C., Bittner, L., Boutte, C., Burgaud, G., de
748 Vargas, C., Decelle, J., del Campo, J., Dolan, J.R., Dunthorn, M., Edvardsen, B., Holzmann,
749 M., Kooistra, W.H.C.F., Lara, E., Le Bescot, N., Logares, R., Mahé, F., Massana, R.,
750 Montresor, M., Morard, R., Not, F., Pawlowski, J., Probert, I., Sauvadet, A.-L., Siano, R.,
751 Stoeck, T., Vaulot, D., Zimmermann, P., Christen, R., 2012. The Protist Ribosomal Reference
752 database (PR2): a catalog of unicellular eukaryote Small Sub-Unit rRNA sequences with
753 curated taxonomy. *Nucleic Acids Research* 41, D597–D604.
754 <https://doi.org/10.1093/nar/gks1160>

755 Hall, J.A., Safi, K., 2001. The impact of in situ Fe fertilisation on the microbial food web in the
756 Southern Ocean. *Deep Sea Research Part II: Topical Studies in Oceanography* 48, 2591–
757 2613. [https://doi.org/10.1016/S0967-0645\(01\)00010-8](https://doi.org/10.1016/S0967-0645(01)00010-8)

758 Henjes, J., Assmy, P., Klaas, C., Verity, P., Smetacek, V., 2007. Response of microzooplankton
759 (protists and small copepods) to an iron-induced phytoplankton bloom in the Southern Ocean
760 (EisenEx). *Deep Sea Research Part I: Oceanographic Research Papers* 54, 363–384.
761 <https://doi.org/10.1016/j.dsr.2006.12.004>

762 Irigoien, X., Flynn, K.J., Harris, R.P., 2005. Phytoplankton blooms: a ‘loophole’ in
763 microzooplankton grazing impact? *Journal of Plankton Research* 27, 313–321.
764 <https://doi.org/10.1093/plankt/fbi011>

765 Irion, S., Jardillier, L., Sassenhagen, I., Christaki, U., 2020. Marked spatio-temporal variations in
766 small phytoplankton structure in contrasted waters of the Southern Ocean (Kerguelen area).
767 *Limnology and Oceanography*. *Limnol Oceanogr* Ino.11555.
768 <https://doi.org/10.1002/lno.11555>

769 Irion, S., Christaki, U., Berthelot, U., L’Helghen, S., Jardillier, L., Small phytoplankton contribute
770 greatly to CO₂-fixation after the diatom bloom in the Southern Ocean 2021. *ISME journal*,
771 <https://doi.org/10.1038/s41396-021-00915-z> (in press)

- 772 Jeong, H.J., Yoo, Y.D., Kim, J.S., Seong, K.A., Kang, N.S., Kim, T.H., 2010. Growth, feeding and
773 ecological roles of the mixotrophic and heterotrophic dinoflagellates in marine planktonic
774 food webs. *Ocean Sci. J.* 45, 65–91. <https://doi.org/10.1007/s12601-010-0007-2>
- 775 Jeong, H.J., You, J.H., Lee, K.H., Kim, S.J., Lee, S.Y., 2018. Feeding by common heterotrophic
776 protists on the mixotrophic alga *Gymnodinium smaydae* (Dinophyceae), one of the fastest
777 growing dinoflagellates. *J. Phycol.* 54, 734–743. <https://doi.org/10.1111/jpy.12775>
- 778 Karayanni, H., Christaki, U., Van Wambeke, F., Thyssen, M., Denis, M., 2008. Heterotrophic
779 nanoflagellate and ciliate bacterivorous activity and growth in the northeast Atlantic Ocean: a
780 seasonal mesoscale study. *Aquat. Microb. Ecol.* 51, 169–181.
781 <https://doi.org/10.3354/ame01181>
- 782 Kenkel, N.C., 2006. On selecting an appropriate multivariate analysis. *Can. J. Plant Sci.* 86, 663–676.
783 <https://doi.org/10.4141/P05-164>
- 784 Kiørboe, T., Visser, A., 1999. Predator and prey perception in copepods due to hydromechanical
785 signals. *Mar. Ecol. Prog. Ser.* 179, 81–95. <https://doi.org/10.3354/meps179081>
- 786 Kofoed, C.A., Campbell, A.S., 1929. A Conspectus of the Marine and Freshwater Ciliata Belonging
787 to the suborder Tintinnoinea, with Descriptions of New Species Principally from the Agassiz
788 Expedition to the Eastern Tropical Pacific 1904-1905. University of California Publications in
789 Zoology, Berkley, Calif. vol. pp. 403.
- 790 Landry, M.R., Hassett, R.P., 1982. Estimating the grazing impact of marine micro-zooplankton.
791 *Marine Biology* 67, 283–288. <https://doi.org/10.1007/BF00397668>
- 792 Landry, M.R., Selph, K.E., Décima, M., Gutiérrez-Rodríguez, A., Stukel, M.R., Taylor, A.G.,
793 Pasulka, A.L., 2016. Phytoplankton production and grazing balances in the Costa Rica Dome.
794 *J. Plankton Res.* 38, 366–379. <https://doi.org/10.1093/plankt/fbv089>
- 795 Lasbleiz, M., Leblanc, K., Blain, S., Ras, J., Cornet-Barthaux, V., Hélias Nunige, S., Quéguiner, B.,
796 2014. Pigments, elemental composition (C, N, P, and Si), and stoichiometry of particulate
797 matter in the naturally iron fertilized region of Kerguelen in the Southern Ocean.
798 *Biogeosciences* 11, 5931–5955. <https://doi.org/10.5194/bg-11-5931-2014>
- 799 Lasbleiz, M., Leblanc, K., Armand, L.K., Christaki, U., Georges, C., Obernosterer, I., Quéguiner, B.,
800 2016. Composition of diatom communities and their contribution to plankton biomass in the
801 naturally iron-fertilized region of Kerguelen in the Southern Ocean. *FEMS Microbiol Ecol*
802 92. <https://doi.org/10.1093/femsec/fiw171>
- 803 Lawrence, C., Menden-Deuer, S., 2012. Drivers of protistan grazing pressure: seasonal signals of
804 plankton community composition and environmental conditions. *Mar. Ecol. Prog. Ser.* 459,
805 39–52. <https://doi.org/10.3354/meps09771>

806 Lê, S., Josse, J., Husson, F., 2008. FactoMineR : An R Package for Multivariate Analysis. *J. Stat.*
807 *Soft.* 25. <https://doi.org/10.18637/jss.v025.i01>

808 Lee, K.H., Jeong, H.J., Jang, T.Y., Lim, A.S., Kang, N.S., Kim, J.-H., Kim, K.Y., Park, K.-T., Lee,
809 K., 2014. Feeding by the newly described mixotrophic dinoflagellate *Gymnodinium smaydae*:
810 Feeding mechanism, prey species, and effect of prey concentration. *Journal of Experimental*
811 *Marine Biology and Ecology* 459, 114–125. <https://doi.org/10.1016/j.jembe.2014.05.011>

812 Letunic, I., Bork, P., 2016. Interactive tree of life (iTOL) v3: an online tool for the display and
813 annotation of phylogenetic and other trees. *Nucleic Acids Res* 44, W242–W245.
814 <https://doi.org/10.1093/nar/gkw290>

815 Lynn, D.H., Montagnes, D.J.S., 1988. Taxonomic Descriptions of Some Conspicuous Species of
816 Strobilidiine Ciliates (Ciliophora: Choreotrichida) from the Isles of Shoals, Gulf of Maine.
817 *Journal of the Marine Biological Association of the United Kingdom* 68, 639–658.
818 <https://doi.org/10.1017/S0025315400028770>

819 Mackey, M., Mackey, D., Higgins, H., Wright, S., 1996. CHEMTAX - a program for estimating class
820 abundances from chemical markers: application to HPLC measurements of phytoplankton.
821 *Mar. Ecol. Prog. Ser.* 144, 265–283. <https://doi.org/10.3354/meps144265>

822 McMinn, A., Scot, F. J., 2005. Dinoflagellates, in: Scott, F. J., Marchant H.W. (Eds), *Antarctic*
823 *marine protists*. ABRS and AAD Publishers, Canberra, pp. 202-250.

824 McMurdie, P.J., Holmes, S., 2013. phyloseq: An R Package for Reproducible Interactive Analysis
825 and Graphics of Microbiome Census Data. *PLoS ONE* 8, e61217.
826 <https://doi.org/10.1371/journal.pone.0061217>

827 Medinger, R., Nolte, V., Pandey, R.V., Jost, S., Ottenwälder, B., Schlötterer, C., Boenigk, J., 2010.
828 Diversity in a hidden world: potential and limitation of next-generation sequencing for
829 surveys of molecular diversity of eukaryotic microorganisms. *Molecular Ecology* 19, 32–40.
830 <https://doi.org/10.1111/j.1365-294X.2009.04478.x>

831 Menden-Deuer, S., Lawrence, C., Franzè, G., 2018. Herbivorous protist growth and grazing rates at
832 in situ and artificially elevated temperatures during an Arctic phytoplankton spring bloom.
833 *PeerJ* 6, e5264. <https://doi.org/10.7717/peerj.5264>

834 Menden-Deuer, S., Lessard, E.J., 2000. Carbon to volume relationships for dinoflagellates, diatoms,
835 and other protist plankton. *Limnol. Oceanogr.* 45, 569–579.
836 <https://doi.org/10.4319/lo.2000.45.3.0569>

837 Mordret, S., Piredda, R., Vaultot, D., Montresor, M., Kooistra, W.H.C.F., Sarno, D., 2018. DINOREF :
838 A curated dinoflagellate (Dinophyceae) reference database for the 18S rRNA gene. *Mol Ecol*
839 *Resour* 18, 974–987. <https://doi.org/10.1111/1755-0998.12781>

840 Morison, F., Menden-Deuer, S., 2018. Seasonal similarity in rates of protistan herbivory in fjords
841 along the Western Antarctic Peninsula. *Limnol. Oceanogr.* 63, 2858–2876.
842 <https://doi.org/10.1002/lno.11014>

843 Mosseri, J., Quéguiner, B., Armand, L., Cornet-Barthaux, V., 2008. Impact of iron on silicon
844 utilization by diatoms in the Southern Ocean: A case study of Si/N cycle decoupling in a
845 naturally iron-enriched area. *Deep Sea Research Part II: Topical Studies in Oceanography* 55,
846 801–819. <https://doi.org/10.1016/j.dsr2.2007.12.003>

847 Neuer, S., Cowles, T., 1994. Protist herbivory in the Oregon upwelling system. *Mar. Ecol. Prog. Ser.*
848 113, 147–162. <https://doi.org/10.3354/meps113147>

849 Obernosterer, I., Christaki, U., Lefèvre, D., Catala, P., Van Wambeke, F., Lebaron, P., 2008. Rapid
850 bacterial mineralization of organic carbon produced during a phytoplankton bloom induced
851 by natural iron fertilization in the Southern Ocean. *Deep Sea Research Part II: Topical Studies*
852 *in Oceanography* 55, 777–789. <https://doi.org/10.1016/j.dsr2.2007.12.005>

853 Obiol, A., Giner, C.R., Sánchez, P., Duarte, C.M., Acinas, S.G., Massana, R., 2020. A metagenomic
854 assessment of microbial eukaryotic diversity in the global ocean. *Mol Ecol Resour* 20, 1755–
855 0998.13147. <https://doi.org/10.1111/1755-0998.13147>

856 Pawlowski, J., Audic, S., Adl, S., Bass, D., Belbahri, L., Berney, C., Bowser, S.S., Cepicka, I.,
857 Decelle, J., Dunthorn, M., Fiore-Donno, A.M., Gile, G.H., Holzmann, M., Jahn, R., Jirků, M.,
858 Keeling, P.J., Kostka, M., Kudryavtsev, A., Lara, E., Lukeš, J., Mann, D.G., Mitchell, E.A.D.,
859 Nitsche, F., Romeralo, M., Saunders, G.W., Simpson, A.G.B., Smirnov, A.V., Spouge, J.L.,
860 Stern, R.F., Stoeck, T., Zimmermann, J., Schindel, D., de Vargas, C., 2012. CBOL Protist
861 Working Group: Barcoding Eukaryotic Richness beyond the Animal, Plant, and Fungal
862 Kingdoms. *PLoS Biol* 10, e1001419. <https://doi.org/10.1371/journal.pbio.1001419>

863 Petz, W., 2005. Ciliates. in: Scott, F. J., Marchant, H.J. (Eds.), *Antarctic Marine Protists*. ABRIS and
864 AAD Publishers, Canberra, pp. 563.

865 Pollard, R., Sanders, R., Lucas, M., Statham, P., 2007. The Crozet Natural Iron Bloom and Export
866 Experiment (CROZEX). *Deep Sea Research Part II: Topical Studies in Oceanography* 54,
867 1905–1914. <https://doi.org/10.1016/j.dsr2.2007.07.023>

868 Pollard, R.T., Salter, I., Sanders, R.J., Lucas, M.I., Moore, C.M., Mills, R.A., Statham, P.J., Allen,
869 J.T., Baker, A.R., Bakker, D.C.E., Charette, M.A., Fielding, S., Fones, G.R., French, M.,
870 Hickman, A.E., Holland, R.J., Hughes, J.A., Jickells, T.D., Lampitt, R.S., Morris, P.J.,
871 Nédélec, F.H., Nielsdóttir, M., Planquette, H., Popova, E.E., Poulton, A.J., Read, J.F.,
872 Seeyave, S., Smith, T., Stinchcombe, M., Taylor, S., Thomalla, S., Venables, H.J.,
873 Williamson, R., Zubkov, M.V., 2009. Southern Ocean deep-water carbon export enhanced by

874 natural iron fertilization. *Nature* 457, 577–580. <https://doi.org/10.1038/nature07716>

875 Poulton, A.J., Mark Moore, C., Seeyave, S., Lucas, M.I., Fielding, S., Ward, P., 2007. Phytoplankton
876 community composition around the Crozet Plateau, with emphasis on diatoms and
877 Phaeocystis. *Deep Sea Research Part II: Topical Studies in Oceanography* 54, 2085–2105.
878 <https://doi.org/10.1016/j.dsr2.2007.06.005>

879 Putt, M., Stoecker, D.K., 1989. An experimentally determined carbon : volume ratio for marine
880 “oligotrichous” ciliates from estuarine and coastal waters. *Limnol. Oceanogr.* 34, 1097–1103.
881 <https://doi.org/10.4319/lo.1989.34.6.1097>

882 Quéguiner, B., 2013. Iron fertilization and the structure of planktonic communities in high nutrient
883 regions of the Southern Ocean. *Deep Sea Research Part II: Topical Studies in Oceanography*
884 90, 43–54. <https://doi.org/10.1016/j.dsr2.2012.07.024>

885 Ras, J., Claustre, H., Uitz, J., 2008. Spatial variability of phytoplankton pigment distributions in the
886 Subtropical South Pacific Ocean: comparison between in situ and predicted data.
887 *Biogeosciences* 5, 353–369. <https://doi.org/10.5194/bg-5-353-2008>

888 Rose, J.M., Fitzpatrick, E., Wang, A., Gast, R.J., Caron, D.A., 2013. Low temperature constrains
889 growth rates but not short-term ingestion rates of Antarctic ciliates. *Polar Biol* 36, 645–659.
890 <https://doi.org/10.1007/s00300-013-1291-y>

891 Saito, H., Suzuki, K., Hinuma, A., Ota, T., Fukami, K., Kiyosawa, H., Saino, T., Tsuda, A., 2005.
892 Responses of microzooplankton to in situ iron fertilization in the western subarctic Pacific
893 (SEEDS). *Progress in Oceanography* 64, 223–236.
894 <https://doi.org/10.1016/j.pocean.2005.02.010>

895 Saito, H., Ota, T., Suzuki, K., Nishioka, J., Tsuda, A., 2006. Role of heterotrophic dinoflagellate
896 *Gyrodinium* sp. in the fate of an iron induced diatom bloom. *Geophys. Res. Lett.* 33, L09602.
897 <https://doi.org/10.1029/2005GL025366>

898 Sarthou, G., Vincent, D., Christaki, U., Obernosterer, I., Timmermans, K.R., Brussaard, C.P.D.,
899 2008. The fate of biogenic iron during a phytoplankton bloom induced by natural fertilisation:
900 Impact of copepod grazing. *Deep Sea Research Part II: Topical Studies in Oceanography* 55,
901 734–751. <https://doi.org/10.1016/j.dsr2.2007.12.033>

902 Sassenhagen, I., Irion, S., Jardillier, L., Moreira, D., Christaki, U., 2020. Protist Interactions and
903 Community Structure During Early Autumn in the Kerguelen Region (Southern Ocean).
904 *Protist* 171, 125709. <https://doi.org/10.1016/j.protis.2019.125709>

905 Schiller, J., 1931–1937: Dinoflagellatae (Peridinineae) in monographischer Behandlung. in:
906 Rabenhorst, L. (Eds.), *Kryptogamen-Flora von Deutschland, Österreichs und der Schweiz*.
907 Akad. Verlag., Leipzig. Vol. 10 (3): Teil 1 (1–3) (1931–1933): Teil 2 (1–4) (1935–1937).

908 Schmoker, C., Hernández-León, S., Calbet, A., 2013. Microzooplankton grazing in the oceans:
909 impacts, data variability, knowledge gaps and future directions. *Journal of Plankton Research*
910 35, 691–706. <https://doi.org/10.1093/plankt/fbt023>

911 Sherr, B.F., Sherr, E.B., Fallon, R.D., 1987. Use of Monodispersed, Fluorescently Labeled Bacteria
912 to Estimate In Situ Protozoan Bacterivory. *Appl. Environ. Microbiol.* 53, 958-965.

913 Sherr, E., Sherr, B., 2007. Heterotrophic dinoflagellates: a significant component of
914 microzooplankton biomass and major grazers of diatoms in the sea. *Mar. Ecol. Prog. Ser.* 352,
915 187–197. <https://doi.org/10.3354/meps07161>

916 Sherr, E., Sherr, B., 2009. Capacity of herbivorous protists to control initiation and development of
917 mass phytoplankton blooms. *Aquat. Microb. Ecol.* 57, 253–262.
918 <https://doi.org/10.3354/ame01358>

919 Smetacek, V., Assmy, P., Henjes, J., 2004. The role of grazing in structuring Southern Ocean pelagic
920 ecosystems and biogeochemical cycles. *Antarctic science* 16, 541–558.
921 <https://doi.org/10.1017/S0954102004002317>

922 Stamatakis, A., 2014. RAxML version 8: a tool for phylogenetic analysis and post-analysis of large
923 phylogenies. *Bioinformatics* 30, 1312–1313. <https://doi.org/10.1093/bioinformatics/btu033>

924 Steinberg, D.K., Landry, M.R., 2017. Zooplankton and the Ocean Carbon Cycle. *Annu. Rev. Mar.*
925 *Sci.* 9, 413–444. <https://doi.org/10.1146/annurev-marine-010814-015924>

926 Stern, R., Kraberg, A., Bresnan, E., Kooistra, W.H.C.F., Lovejoy, C., Montresor, M., Morán, X.A.G.,
927 Not, F., Salas, R., Siano, R., Vaultot, D., Amaral-Zettler, L., Zingone, A., Metfies, K., 2018.
928 Molecular analyses of protists in long-term observation programmes—current status and
929 future perspectives. *Journal of Plankton Research* 40, 519–536.
930 <https://doi.org/10.1093/plankt/fby035>

931 Stoecker, D.K., Capuzzo, J.M., 1990. Predation on Protozoa: its importance to zooplankton. *J*
932 *Plankton Res* 12, 891–908. <https://doi.org/10.1093/plankt/12.5.891>

933 Straile, D., 1997. Gross growth efficiencies of protozoan and metazoan zooplankton and their
934 dependence on food concentration, predator-prey weight ratio, and taxonomic group. *Limnol.*
935 *Oceanogr.* 42, 1375–1385. <https://doi.org/10.4319/lo.1997.42.6.1375>

936 Strom, S., 1991. Growth and grazing rates of the herbivorous dinoflagellate *Gymnodinium* sp. from
937 the open subarctic Pacific Ocean. *Mar. Ecol. Prog. Ser.* 78, 103–113.
938 <https://doi.org/10.3354/meps078103>

939 Strom, S.L., Fredrickson, K.A., 2008. Intense stratification leads to phytoplankton nutrient limitation
940 and reduced microzooplankton grazing in the southeastern Bering Sea. *Deep Sea Research*
941 *Part II: Topical Studies in Oceanography* 55, 1761–1774.

- 942 <https://doi.org/10.1016/j.dsr2.2008.04.008>
- 943 Tomas, C.R., 1997. *Identifying Marine Phytoplankton*. Elsevier, London. pp.858
- 944 Tsuda, A., Takeda, S., Saito, H., Nishioka, J., Kudo, I., Nojiri, Y., Suzuki, K., Uematsu, M., Wells,
945 M.L., Tsumune, D., Yoshimura, T., Aono, T., Aramaki, T., Cochlan, W.P., Hayakawa, M.,
946 Imai, K., Isada, T., Iwamoto, Y., Johnson, W.K., Kameyama, S., Kato, S., Kiyosawa, H.,
947 Kondo, Y., Levasseur, M., Machida, R.J., Nagao, I., Nakagawa, F., Nakanishi, T., Nakatsuka,
948 S., Narita, A., Noiri, Y., Obata, H., Ogawa, H., Oguma, K., Ono, T., Sakuragi, T., Sasakawa,
949 M., Sato, M., Shimamoto, A., Takata, H., Trick, C.G., Watanabe, Y.W., Wong, C.S., Yoshie,
950 N., 2007. Evidence for the grazing hypothesis: Grazing reduces phytoplankton responses of
951 the HNLC ecosystem to iron enrichment in the western subarctic pacific (SEEDS II). *J*
952 *Oceanogr* 63, 983–994. <https://doi.org/10.1007/s10872-007-0082-x>
- 953 Uitz, J., Claustre, H., Griffiths, F.B., Ras, J., Garcia, N., Sandroni, V., 2009. A phytoplankton class-
954 specific primary production model applied to the Kerguelen Islands region (Southern Ocean).
955 *Deep Sea Research Part I: Oceanographic Research Papers* 56, 541–560.
956 <https://doi.org/10.1016/j.dsr.2008.11.006>
- 957 Vargas, C., González, H., 2004. Plankton community structure and carbon cycling in a coastal
958 upwelling system. I. Bacteria, microprotozoans and phytoplankton in the diet of copepods and
959 appendicularians. *Aquat. Microb. Ecol.* 34, 151–164. <https://doi.org/10.3354/ame034151>
- 960 Verity, P.G., Stoecker, D.K., Sieracki, M.E., Nelson, J.R., 1993. Grazing, growth and mortality of
961 microzooplankton during the 1989 North Atlantic spring bloom at 47°N, 18°W. *Deep Sea*
962 *Research Part I: Oceanographic Research Papers* 40, 1793–1814.
963 [https://doi.org/10.1016/0967-0637\(93\)90033-Y](https://doi.org/10.1016/0967-0637(93)90033-Y)
- 964 Wolf, C., Frickenhaus, S., Kiliyas, E.S., Peeken, I., Metfies, K., 2014. Protist community composition
965 in the Pacific sector of the Southern Ocean during austral summer 2010. *Polar Biol* 37, 375–
966 389. <https://doi.org/10.1007/s00300-013-1438-x>

967

968 Figure legends

969 Figure 1. Location of stations Surface Chlorophyll *a* concentrations during MOBYDICK are the
970 monthly means for March 2018 at a resolution of 4 km (Copernicus Marine Service,
971 <http://marine.copernicus.eu/>). The black lines denote 1000 m bathymetry. The approximate position
972 of the highly dynamic polar front (PF, blue line) during February-March 2018 was also drawn
973 according to Pauthenet et al. (2018), gray zone around the polar front indicates variations in its
974 trajectory. The position of the on-plateau A3 and reference HNLC R stations sampled during early

975 spring (KEOPS2 cruise, October-November 2011) are also indicated on this map. KEOPS2 station
976 A3 was named M2 during the MOBYDICK cruise and has the same coordinates.

977

978 Figure 2. Mean profiles of Temperature (°C), Salinity and Chl-*a* (derived from in vivo fluorescence)
979 calculated from all the CTDs of each visit to a station. Shadows are standard deviations around the
980 mean of all CTDs sampled at each station.

981

982 Figure 3. Mean contribution and relative contribution of pigments to total Chl. diat=diatoms,
983 prymn=prymnesiophytes, pras=prasinophytes, crypt=cryptophytes, syn=*Synechococcus*,
984 chlor=chlorophytes. A3-1, A3-2 and R: correspond to early spring data (KEOPS2, cruise). Late
985 summer: MOBYDICK cruise.

986

987 Figure 4. Mean integrated abundances and relative abundance of dinoflagellate (DIN) size classes (a,
988 b). Mean integrated abundances and relative abundance of ciliates (CIL) size classes (c, d) Mean
989 integrated biomasses of DIN and CIL (e) and relative biomasses of DIN and CIL (f), in the mixed
990 layer (ML).

991

992 Figure 5. Vertical profiles of dinoflagellates (DIN) and ciliates (CIL) during the MOBYDICK cruise.

993

994 Figure 6. Heatmaps illustrating microscopy (a, b) versus sequencing (c, d) diversity and abundance
995 data for dinoflagellates (DIN) ciliates (CIL) during MOBYDICK. DIN and CIL microscopy data
996 values are the mean integrated abundances of cells in the ML (cells L⁻¹) (a and b, respectively). DIN
997 and CIL sequence data illustrate relative abundance of reads in the 0.2-20 and 20-100 µm size
998 fractions in the class Dinophyceae (c) and, the relative abundance of reads in the 0.2-20 and 20-100
999 µm size fractions in the division Ciliophora (d).

1000

1001 Figure 7. Maximum likelihood trees for dinoflagellate (DIN)(a) and ciliate (CIL)(b) genera.
1002 Bootstrap values >50 are indicated on branches. Tree scales refer to the length of branches and
1003 indicate the mean number of substitutions per site. Genera are coloured by order. a) DIN topology.
1004 Purple = Noctilucales, blue = Gymnodiniales, green = Peridiniales, orange = Gonyaulacales, red =
1005 Dinophysiales, black = individual orders for each genus. b) CIL topology. Green = Tintinnida, red =
1006 Choreotrichia, purple = Colpodea, orange = Hypotrichia, blue = Strombidiida, black = Cyclotrichiida
1007 (Myrionecta), Scuticociliatia, Euplotia (Diophrys, Aspidisca).

1008

1009 Figure 8. Co-inertia analysis (PCA–PCA COIA) between the 16 most abundant DIN+CIL genera and
1010 characteristic pigments. The two Hierarchical Clustering Factor Maps and the two PCA applied to
1011 each table are the intermediate steps of the analysis before the final COIA-Biplot. They are presented
1012 here in order to better follow the text of Section 3.3. Hierarchical Clustering Factor Maps indicate
1013 station groupings according to the DIN and CIL dominant genera (a) and pigments concentrations (b).
1014 Also presented are the results of the Principal Component Analysis (PCA) of DIN+CIL (c) and
1015 pigments (d) with their contribution to the first two principal components, and finally the
1016 synthesized COIA results (e). The *x*-axes show projections of the first 3 PCA components from the
1017 pigments while the *y*-axes show those of the genera (e). The circles represent a view of the rotation
1018 needed to associate the 2 datasets. P-values were calculated using Monte Carlo permutation tests
1019 (1000 permutations). The sample scatterplot shows how far apart the samples were relative to their
1020 pigment and taxonomic variables (e). The beginning of the arrow shows the position of the sample
1021 described by the pigments, and the end by the microzooplankton genera. RV: correlation coefficient
1022 between the 2 tables ('R' for correlation and 'V' for vectorial) (e)

1023 Supplementary Material

1024 Fig. A1. Dilution experiment plots of apparent phytoplankton growth (μ , d^{-1}) as a function of the
1025 fraction of bulk seawater (sieved on 200 μ m) in the dilution series for each station. Linear models
1026 have been associated to their 95% confidence interval (dark grey area). Calculated parameters are
1027 detailed on the plot (Ex). Apparent phytoplankton growth (μ) was obtained from measured chl a
1028 concentrations at each dilution by using the equation $\mu = 1/t * \ln(Cf/C0)$ where *t* is the duration of the
1029 experiment (*d*), *Cf* and *C0* are the final and the initial chl a concentrations. The coefficients *k* and *g*
1030 have been determined from the best fit of the linear model linking apparent phytoplankton growth (μ)
1031 versus the dilution factor of whole seawater, *g* (microzooplankton grazing) being the negative slope
1032 and *k* (phytoplankton growth rate) the intercept of the linear model.

Table 1. Station description, coordinates and depth of the CTD "stock". The depth of the mixed layer (Z_{ML}) is based on a difference in sigma of 0.02 to the surface value. The mean Z_{ML} and Z_e ($Z_e=1\%$ light depth) of all CTD casts performed during the occupation of the stations is given. For the rest of the variables the mean \pm SD is given for the mixed layer. **EARLY SPRING**: Onset of the bloom , KEOPS2 cruise (KErguelen Ocean and Plateau compared Study project, 2011), **LATE SUMMER** post-bloom MOBYDICK cruise (2018) on the plateau and ocean area of Kerguelen. The mean ML depth (Z_{ML}) of all CTD casts performed during the occupation of the stations is given. For the rest of the variables the mean \pm SD is given for the mixed layer except for GCP and NCP which is an integrated value in the ML. KEOPS2 station A3 was named M2 during the MOBYDICK cruise and has the same coordinates (cf Fig. 1). KEOPS 2, data from: Blain et al. 2015, Closset et al. 2014, Christaki et al 2014, Lasbleiz et al. 2016. MOBYDICK data of GCP and NCP for from Christaki et al. submitted. NA: not available

	EARLY SPRING			LATE SUMMER							
	On-plateau		Off-plateau	On-plateau			Off-plateau				
Station	A3-1	A3-2	R	M2-1	M2-2	M2-3	M1	M3-1	M3-3	M4-1	M4-2
dates	20 Oct	16 Nov	26 Nov	6-8 Mar	16-17 Mar	8-9 Mar	3-5 Mar	18-20 Mar	28 Feb- 3 Mar	12-14 Mar	6-8 Mar
Long-Lat (°E,°S)	72.1-50.6	72.1-50.6	50.3-66.7	72.0-50.4	72.0-50.4	72.0-50.4	74.5-49.5	68.0-50.4	68.0-50.4	67.1-52.3	67.1-52.3
Depth (m)	475	528	2450	520	519	527	2723	1000	1700	4186	4300
Z_{ML} (m)	105	168	105	62	61	68	27	65	79	49	87
Z_e (m)	N/A	38 38	92 92	64	61	58	80	93	107	96	100
Chlorophyll a (μ g/L)	0.62 \pm 0.17	2.03 \pm 0.33	0.28 \pm 0.04	0.27 \pm 0.02	0.30 \pm 0.04	0.58 \pm 0.02	0.35 \pm 0.040	0.20 \pm 0.02	0.14 \pm 0.00	0.18 \pm 0.01	0.21 \pm 0.00
NO3- + NO2- (μ M)	29.7 \pm 0.5	26.2 \pm 0.4	26.0 \pm 0.2	21.9 \pm 0.12	21.79 \pm 0.38	21.9 \pm 0.08	25.2 \pm 0.56	23.75 \pm 0.31	23.34 \pm 0.12	25.7 \pm 0.05	24.8 \pm 0.27

PO_4^{3-} (μM)	2.00 ± 0.03	1.78 ± 0.03	1.83 ± 0.03	1.47±0.03	1.50±0.04	1.50±0.00	1.71±0.11	1.65±0.05	1.08±0.92	1.70±0.02	1.71±0.01
$\text{Si}(\text{OH})_4$ (μM)	23.7 ± 0.8	18.9 ± 0.5	12.3 ± 0.3	1.36±0.41	1.72±0.79	2.75±0.27	8.38±2.93	2.89±1.01	2.31±0.04	4.36±0.35	4.80±0.00
GCP (mmol C m^{-2})	N/A	344	134	105	213	83	121	nd	132	187	129
NCP (mmol C m^{-2})	N/A	237	57	30	100	44	52	nd	15	88	106

Table 2 : Dilution experiment derived phytoplankton growth and microzooplankton grazing parameters.

Station	On-plateau			Off-plateau			
	M2-1	M2-2	M2-3	M1	M3-1	M4-1	M4-2
Initial Chl a (10-20m depth, $\mu\text{g L}^{-1}$)	0.30	0.36	0.64	0.35	0.20	0.20	0.26
Phytoplankton growth rate (d^{-1})	0.13 ± 0.03	0.15 ± 0.02	0.26 ± 0.03	0.22 ± 0.02	0.17 ± 0.12	0.08 ± 0.03	0.18 ± 0.09
Microzooplankton grazing rate (d^{-1})	0.34 ± 0.05	0.37 ± 0.04	0.53 ± 0.05	0.28 ± 0.03	0.50 ± 0.20	0.38 ± 0.05	0.43 ± 0.15
Dilution determination coefficient (r^2)	0.86***	0.90***	0.81***	0.89***	0.35*	0.83***	0.45*
Phytoplankton daily production ($\mu\text{g Chl a L}^{-1} \text{d}^{-1}$)	0.04 ± 0.009	0.05 ± 0.008	0.17 ± 0.02	0.08 ± 0.006	0.03 ± 0.02	0.02 ± 0.006	0.05 ± 0.02
Microzooplankton daily consumption ($\mu\text{g Chl a L}^{-1} \text{d}^{-1}$)	0.08 ± 0.01	0.13 ± 0.01	0.33 ± 0.03	0.10 ± 0.01	0.10 ± 0.04	0.07 ± 0.008	0.10 ± 0.04
Grazing pressure (%Chl a production d^{-1})	213.10	231.68	194.06	130.05	287.48	427.88	219.86

*** $p < 0.001$; ** $p < 0.01$; * $p < 0.05$

Table 3. Summary of seasonal characteristics above the plateau of Kerguelen and in HNLC waters calculated for the mixed layer (ML). GCP and NCP: Gross and Net community production (cf. Table 1), phytoplankton, dinoflagellates (DIN), ciliates (CIL) dominant genera.

	Productivity regime (GCP)	Community Respiration	DIN+CIL biomass	Phytoplankton	DIN	CIL	DIN+CIL carbon demand* as a % of GCP and NCP
Kerguelen Bloom	mmol C m ⁻² d ⁻¹	% of GCP	mmol C m ⁻²				
Early spring	High ¹ (344)	Low ¹ 30%	High (116)	<i>Chaetoceros</i> <i>Thalassiosira</i> some <i>Phaeocystis</i> colonies ^{3,4}	<i>Gymnodinium</i> , <i>Protoperdinium</i> <i>Gyrodinium</i> ^{4,6}	<i>Strombidium</i> <i>Acanthostomella</i> <i>norvegica</i> <i>Codonellopsis</i> <i>soyai</i> ^{4,6}	18 % GCP 25% NCP (A3-2)
Late summer	Moderate (134) ²	Moderate ² 57 %	low (15.4)	<i>Corethron</i> , <i>Phaeocystis</i> free cells <i>Micromonas</i> ⁵	<i>Gymnodinium</i> <i>Gyrodinium</i> <i>Prorocentrum</i>	<i>Lohmaniella oviformis</i> , <i>Strombidium</i>	5.3±2.4% GCP 14±9.8% NCP (mean±sd of the 3 visits at M2)
HNLC							
Early spring	Moderate (59) ¹	Moderate ¹ 57%	low (17)	<i>Phaeocystis</i> <i>Fragilariopsis</i> ^{3,4}	<i>Gymnodinium</i> <i>Gyrodinium</i> <i>Scripsiella</i> ^{4,6}	<i>Strombidium</i> <i>Codonellopsis soyai</i> ^{4,6}	3 % GCP 8% NCP (R)
Late summer mean±sd of	Moderate (132) ²	High ² 89%	low (16)	<i>Phaeocystis</i> free cells small diatoms	<i>Gymnodinium</i> <i>Scripsiella</i>	<i>Cymatocylis antarctica</i> , <i>Lohmaniella oviformis</i>	3.9±1.8 % GCP 6.8±2.2% NCP

M1, M4-1, M4-2 and M3-3				Pelagophytes ⁵	<i>Gyrodinium</i>		(mean±sd of M1, M4-1, M4-2) 5.2% GCP 46% NCP (M3-3)
-------------------------	--	--	--	---------------------------	-------------------	--	--

*Carbon demand is estimated based on biomass, 30% growth efficiency of (Bjørnsen and Kuparinen, 1991; Verity et al. 1993; Neuer and Cowles, 1994; Karayanni et al. 2008) and $\mu=0.2 \text{ d}^{-1}$ corresponding roughly population generation time of about 3 days (Bjørnsen and Kuparinen, 1991; Verity et al. 1993; Neuer and Cowles, 1994; Karayanni et al. 2008).

1. Christaki et al. 2014; 2. Christaki et al. submitted; 3. Lasbleiz et al. 2016; 4. Georges et al. 2014; 5. Irion et al. 2020; 6. Christaki et al. 2015

Table A1. Significant Pearson correlation between co-inertia axes and variables are highlighted with bold letters (p<0.05)

	axe1	axe2	axe3
Gymnodinium	-0.50563510	0.304129663	-0.67727811
Gyrodinium	0.49828359	0.481226933	-0.45085253
Scrippsiella	-0.91491628	-0.003383030	-0.12224026
Prorocentrum	-0.52196271	-0.100576427	-0.46555616
Amphidinium	0.12412553	0.694065230	-0.10313589
Katodinium	-0.56273600	0.207027089	-0.35686930

Protoperidinium	0.35535326	0.706082523	0.29514842
Triplos	0.15099031	-0.389365386	-0.66223964
Lohmaniella	-0.73329229	-0.319589603	-0.54423781
Strombidium	-0.27722418	0.564209822	-0.64544930
Cymatocylis	-0.41318569	0.168130159	0.21346582
Leegaardiella	-0.59748443	0.008128098	-0.65963309
Codonelepis	-0.07381567	-0.392015027	-0.33990282
Salpingella	-0.73867635	-0.083404745	0.02006962
Laboea	0.14926345	-0.375836980	-0.59724940
Myrionecta	0.72419475	0.532171341	0.07215646

	axe1	axe2	axe3
diat	0.9076259	-0.08972795	-0.20646614
prymn	-0.1780910	-0.71742385	-0.34364613
pras	0.5544056	-0.83415468	-0.01453556
crypt	0.8845281	-0.45060719	-0.13261950
Syn	0.7408795	-0.03714631	-0.71035252
chlor	0.3045928	0.44763322	-0.81309706
Chla	0.9186115	-0.17271963	-0.24602134

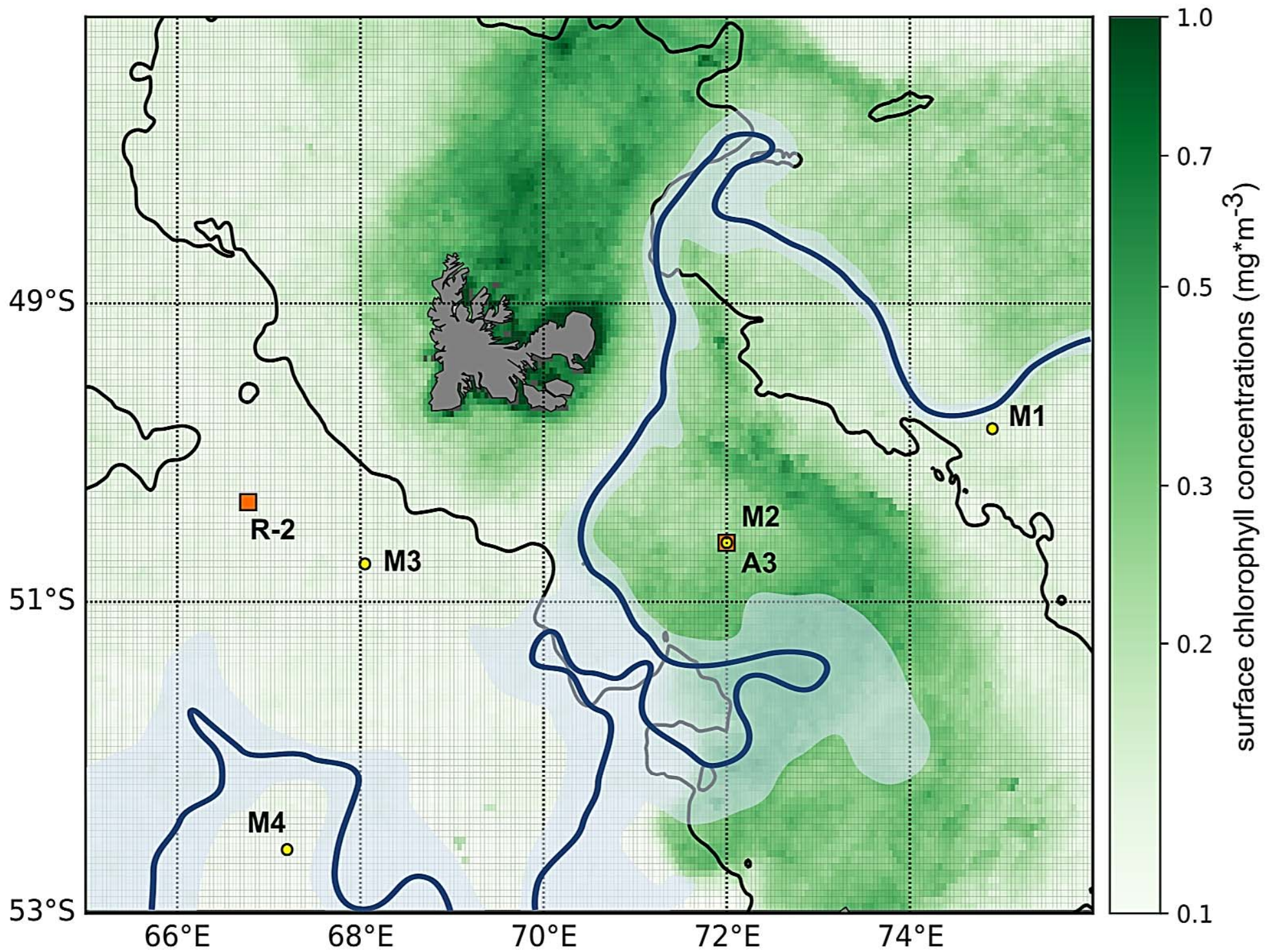
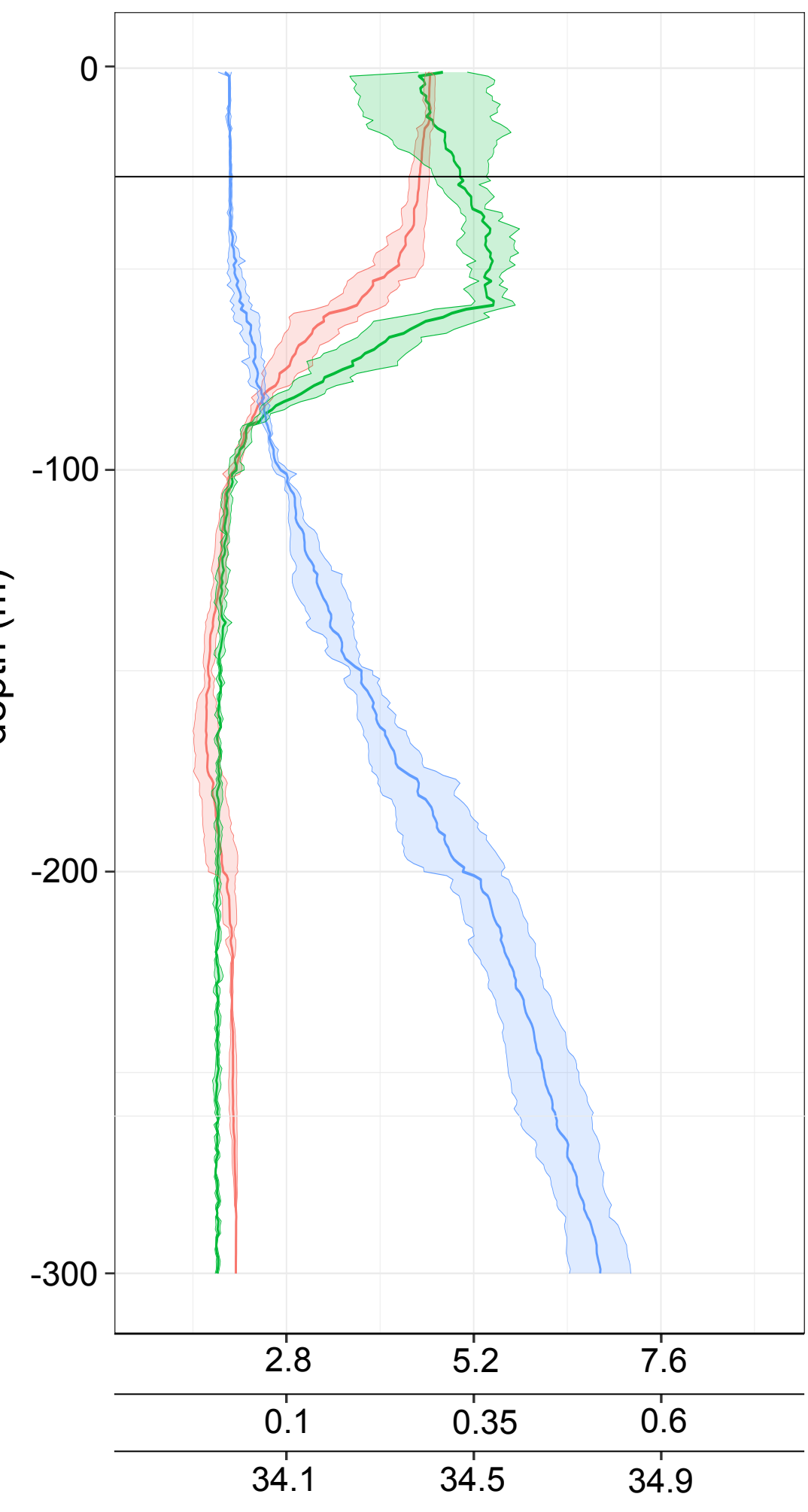
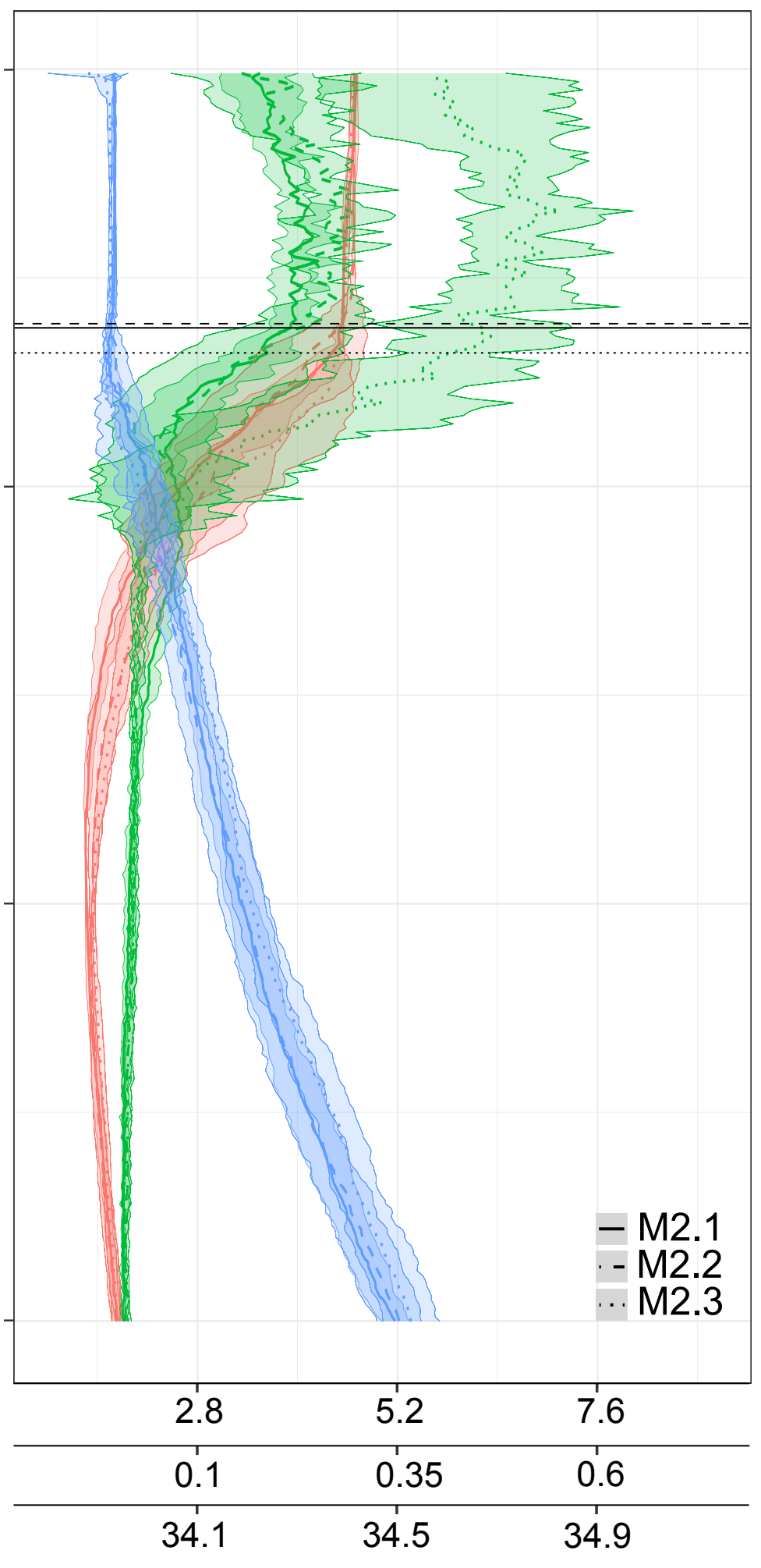


Figure 1

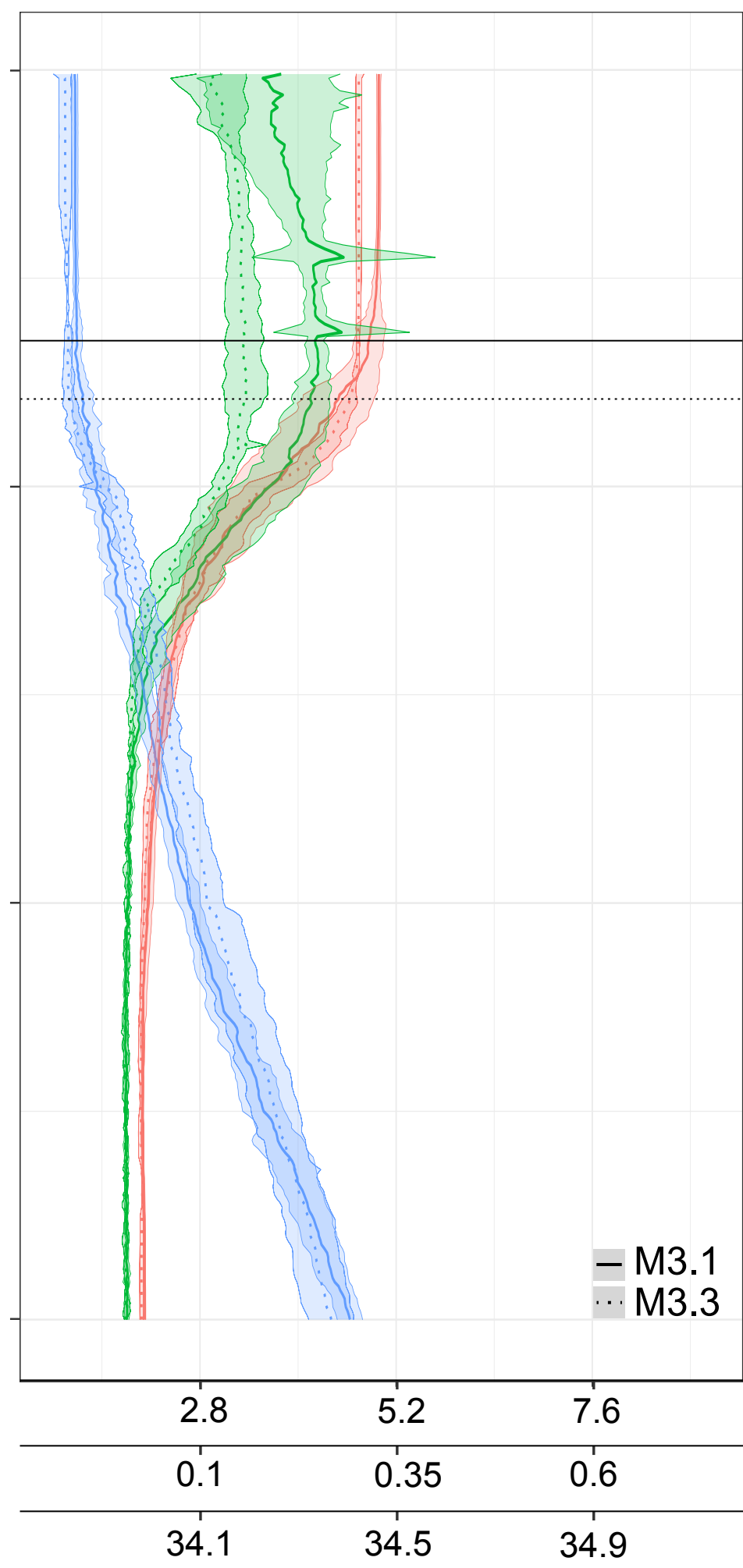
M1



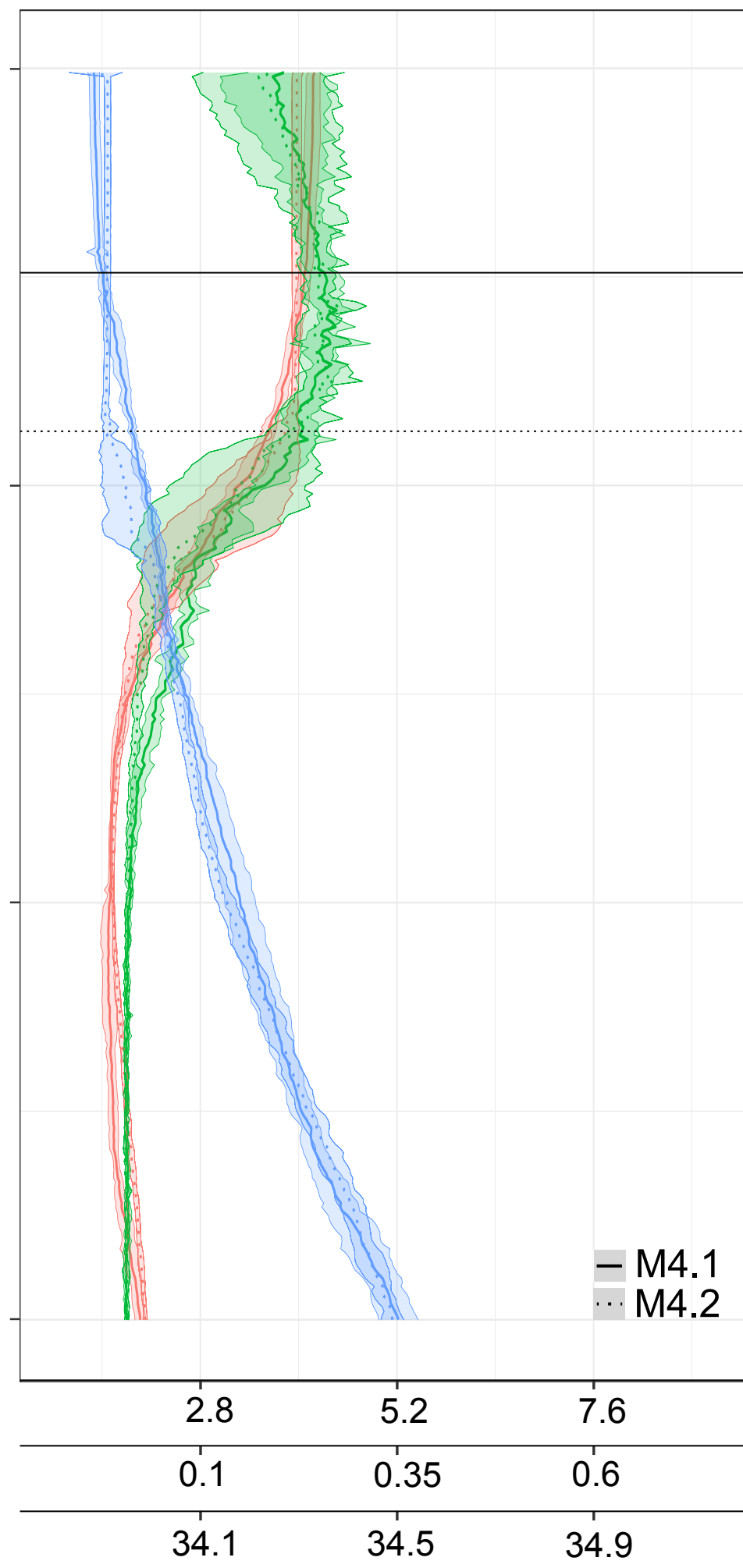
M2



M3



M4



— temperature (°C)
 — salinity
 — Chl a (µg L⁻¹)
 — depth of mixed layer

— M2.1
 - - M2.2
 ··· M2.3

— M3.1
 ··· M3.3

— M4.1
 ··· M4.2

temperature (°C)
 Chl a (µg L⁻¹)
 salinity

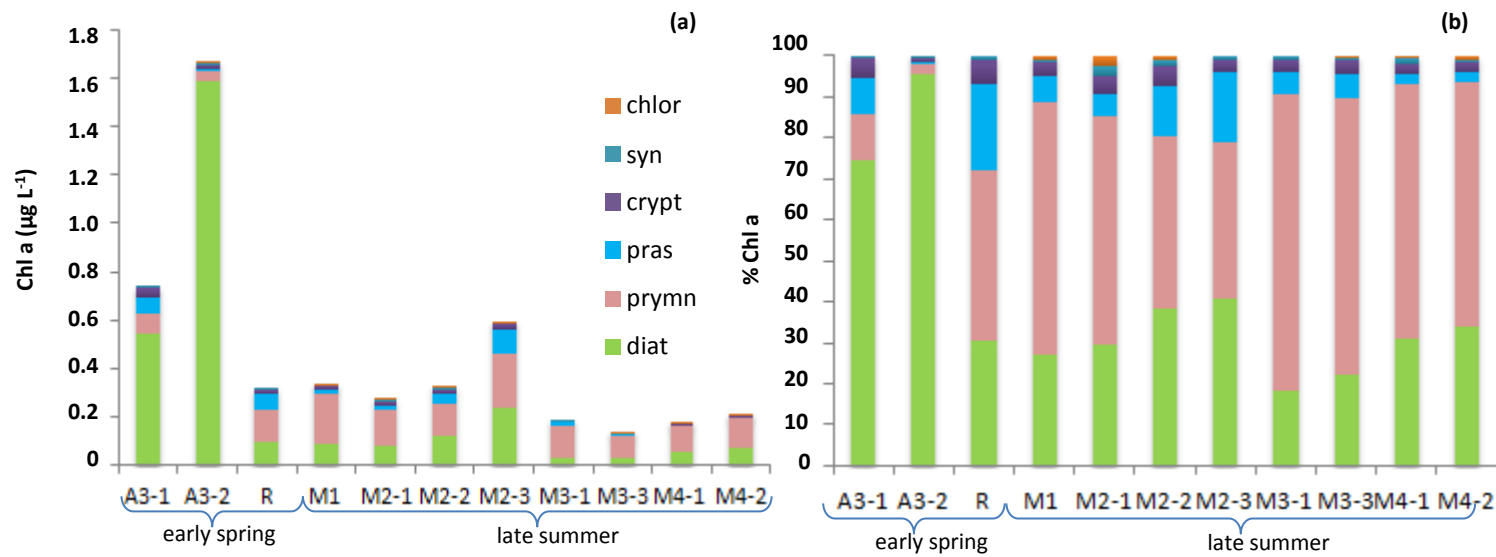


Figure 3

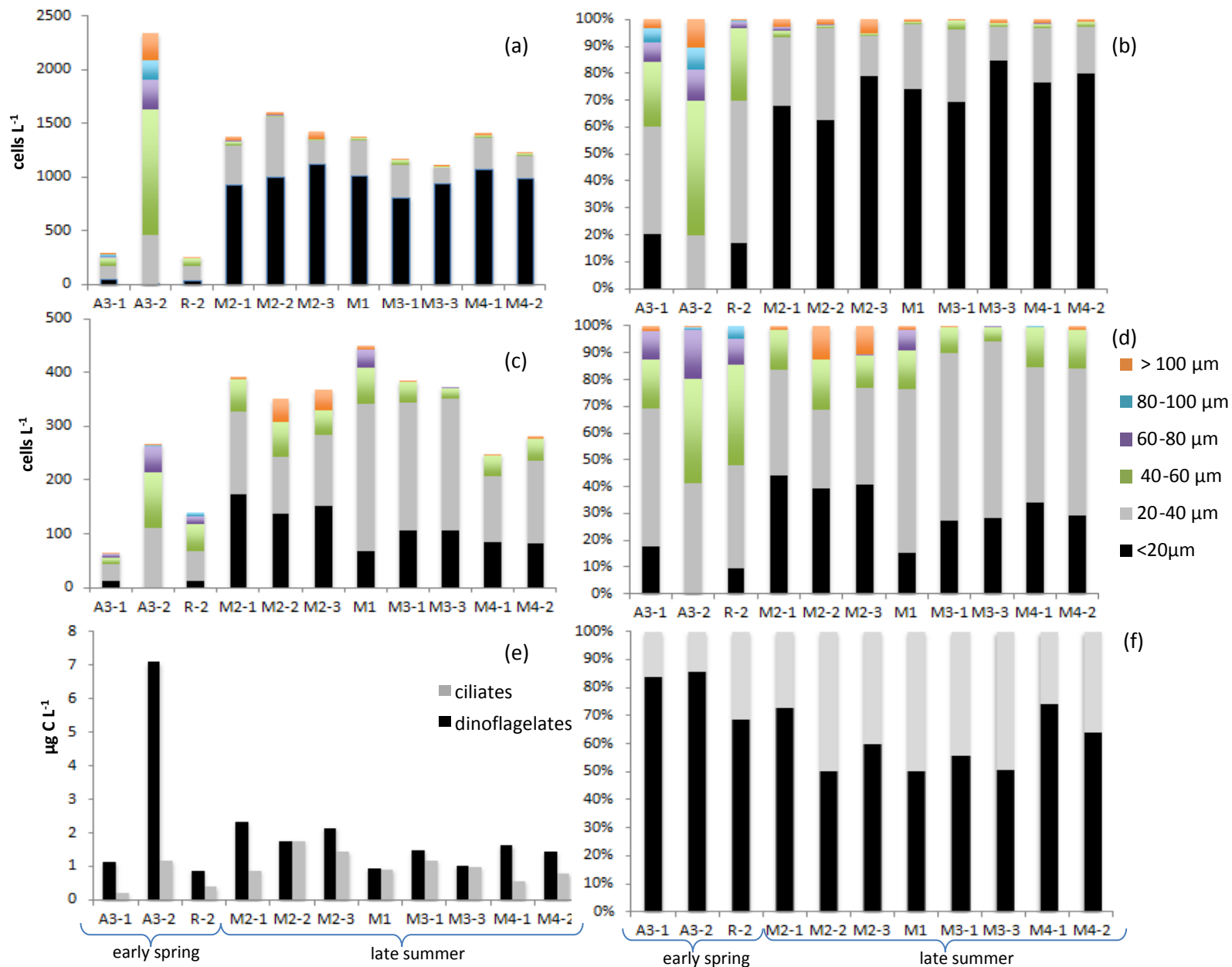


Figure 4

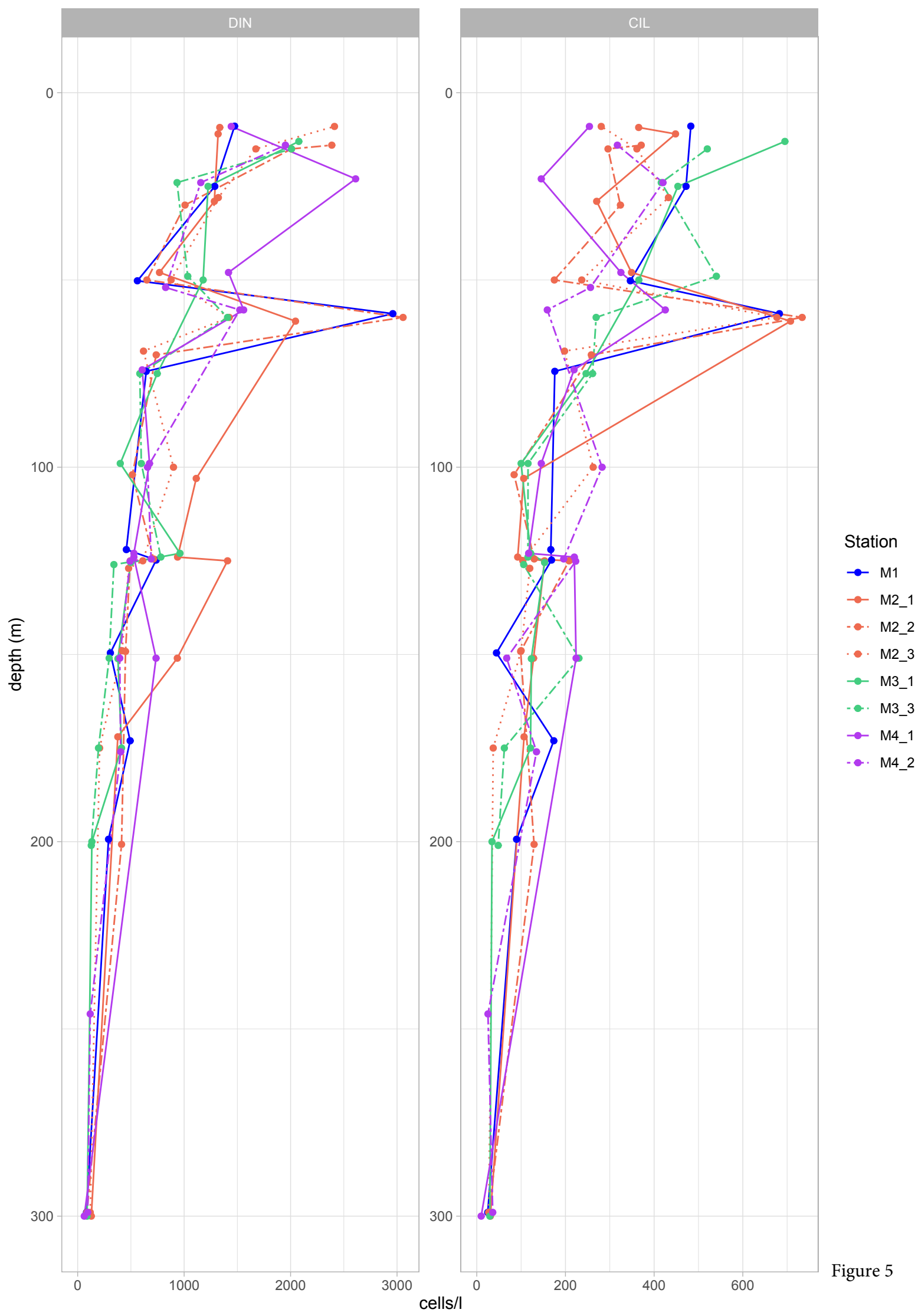


Figure 5

(a)

Amphidinium -	38	85	22	85	24	49	82	67
Amphidinium crassum -	41	40	46	0	2	0	6	0
Dinophysis -	5	0	19	0	0	0	0	0
Gymnodinium -	749	1015	1010	841	1051	804	1265	726
Gyrodinium -	89	251	69	19	87	23	109	32
Gyrodinium fusiforme -	1	0	0	0	0	1	0	11
Gyrodinium spirale -	19	3	3	7	0	0	2	6
Heterocapsa -	0	0	5	0	3	0	11	0
Karodinium -	1	3	0	3	5	0	0	8
Katodinium -	53	22	24	32	47	49	126	36
Oxytoxum -	1	8	2	0	3	0	3	4
Podolampas -	0	0	0	0	0	0	0	1
Pronoctiluca pelagica -	1	0	1	0	0	0	4	1
Proteroperidinium -	36	73	9	10	43	122	33	199
Proteroperidinium antarcticum -	44	0	0	0	28	0	0	0
Proteroperidinium bipes -	1	0	0	0	6	13	0	4
Proteroperidinium cerasus -	0	0	0	0	0	0	0	0
Proteroperidinium depressum -	0	2	1	0	0	0	3	6
Prorocentrum compressum -	31	254	82	163	41	136	106	70
Scrippsiella -	57	88	36	221	167	140	106	131
Torodinium robustum -	46	14	29	39	51	4	15	27
Tripos incisus -	1	0	20	0	0	0	0	0
Tripos lineatus/pentagonus complex -	49	24	51	0	0	2	14	6
	M2-1 -	M2-2 -	M2-3 -	M1 -	M3-1 -	M3-3 -	M4-1 -	M4-2 -

(b)

Codoneopsis soyai -	39	42	12	14	29	3	7	32
Cymatocyclus antarctica -	4	31	41	79	210	164	11	58
Cymatocyclus calysiformis -	2	0	0	0	0	1	0	4
Laboea strobila -	7	47	40	1	1	0	3	6
Leegardiella -	50	52	36	25	52	45	38	35
Lohmaniella oviformis -	112	99	136	177	103	115	35	68
Myrionecta -	11	12	7	0	7	5	8	1
Myrionecta pulex -	0	0	0	7	2	2	3	2
Salpingella acuminata -	2	4	8	62	40	12	13	19
Scuticociliate -	2	0	1	0	4	0	0	0
Strombidium -	34	26	30	41	68	25	56	40
Strombidium antarcticum -	34	10	8	0	0	18	9	2
Strombidium conicum -	14	2	6	0	0	0	0	7
Strombidium sulcatum -	20	17	6	1	3	1	26	2
Strobilidium -	0	18	6	43	0	20	6	0
Tontonia -	18	1	10	26	2	19	0	2
	M2-1 -	M2-2 -	M2-3 -	M1 -	M3-1 -	M3-3 -	M4-1 -	M4-2 -

(c)

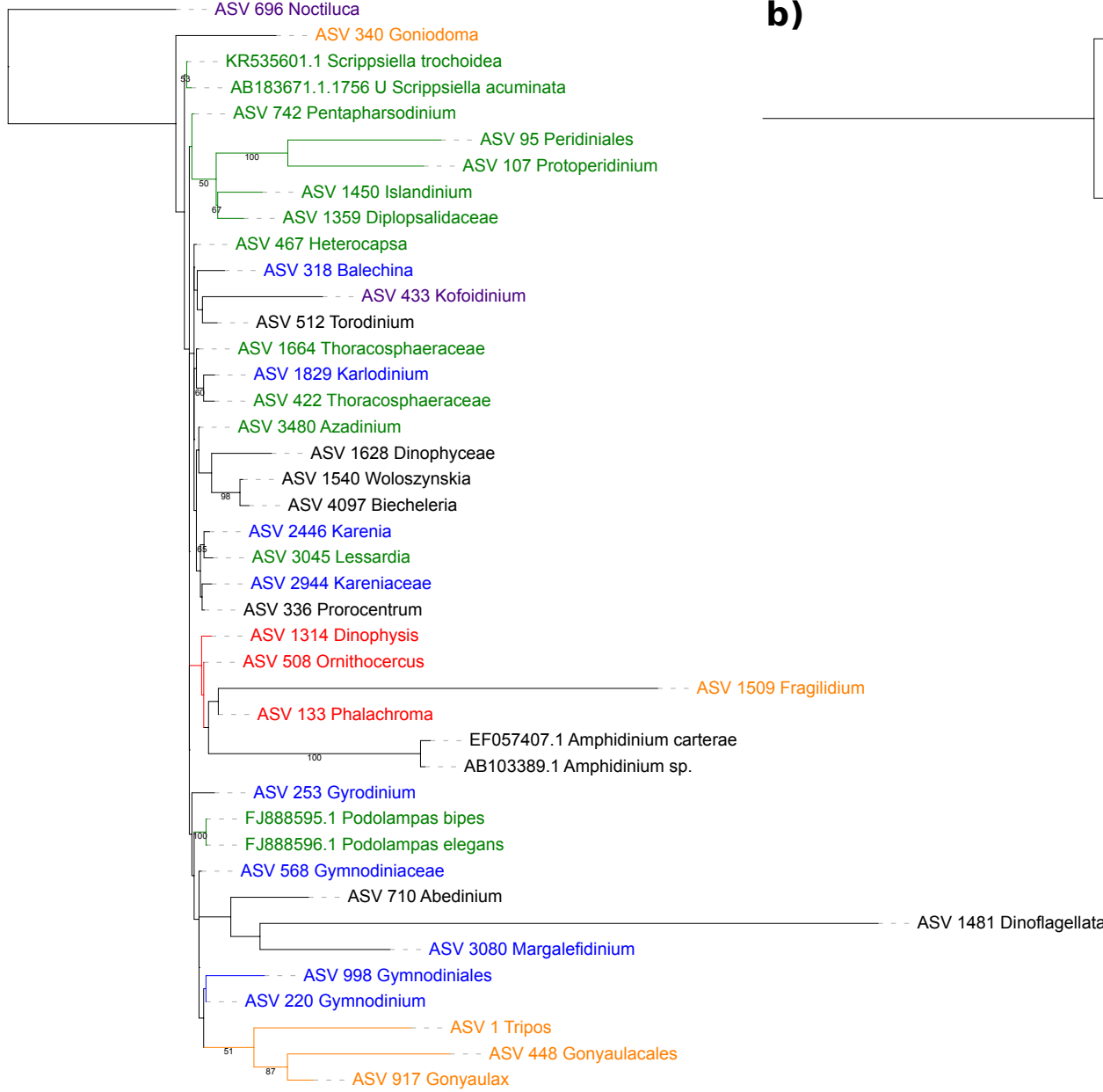
	0-2-20				20-100			
Noctiluca -	0	0	0	0	0	0	0	0
Kofoidinium -	0	0	0	1	0	0	0	0
Torodinium -	2	2	1	2	1	4	2	2
Balechina -	0	1	0	0	0	1	0	0
Azadinium -	0	0	0	0	0	0	0	0
o_Dinophyceae_X_ASV_1628 -	0	0	0	0	0	0	0	0
Woloszynskia -	0	0	0	2	1	0	1	0
f_Kareniaeae_ASV_2944 -	0	0	0	0	0	0	0	0
Prorocentrum -	13	19	23	20	7	18	14	22
Lessardia -	0	0	0	0	0	0	0	0
Karenia -	0	0	0	0	0	0	0	0
Heterocapsa -	1	1	5	4	1	3	7	3
f_Thoracosphaeraeae_ASV_1664 -	0	0	1	0	0	0	0	0
Thoracosphaeraeae_X -	9	1	0	0	1	0	1	3
Karodinium -	0	0	0	2	0	1	2	1
Gyrodinium -	3	26	14	15	12	9	13	10
f_Gymnodiniaceae_ASV_568 -	0	0	1	2	1	0	2	1
Margalefidinium -	0	0	0	0	0	0	0	0
Abedinium -	0	0	0	0	0	0	0	0
Gymnodinium -	25	16	20	27	19	11	22	21
o_Gymnodiniales_ASV_998 -	0	0	1	0	0	1	0	0
Tripos -	39	26	26	15	43	44	26	28
Gonyaulax -	1	0	0	0	0	0	0	0
o_Gonyaulacales_ASV_448 -	0	0	0	0	0	0	0	8
Dinophysis -	0	0	0	0	0	0	0	0
Ornithocercus -	0	0	0	0	0	0	0	0
Phalochroma -	3	3	2	7	3	3	2	2
Goniodoma -	0	0	0	0	0	0	0	0
Pentaptharsodinium -	0	0	0	0	0	2	1	0
o_Peridiniales_ASV_95 -	0	1	2	3	1	1	2	1
Proteroperidinium -	2	3	3	1	5	3	3	3
	M2-1 -	M2-2 -	M2-3 -	M1 -	M3-1 -	M3-3 -	M4-1 -	M4-2 -

(d)

	0-2-20				20-100			
Dictyocystidae_X-TIN_03_X -	4	3	1	6	2	2	4	3
o_Tintinnida_ASV_1312 -	0	0	0	0	0	0	0	0
f_Xystonellidae_ASV_6 -	8	13	4	9	19	15	5	6
c_Spirotrichea_ASV_1667 -	0	0	0	0	0	0	0	0
Pelagostrobilidium -	0	0	0	0	0	0	0	0
Eutintinnidae_X -	0	0	0	1	1	1	1	1
Amphorellopsis -	0	0	0	0	0	0	0	0
Salpingella -	2	3	1	2	4	2	1	7
Tintinnidae_X -	3	2	2	6	7	17	8	20
Strobilidiidae_I_X -	1	0	0	0	0	0	0	0
Strobilidiidae_J_X -	0	0	0	0	0	0	0	0
Tintinnidium -	0	0	0	0	0	0	0	0
Strobilidiidae_A_X -	0	0	0	0	0	0	0	0
Rimostrombidium_A -	0	0	0	0	0	0	0	0
Strobilidiidae_B_X -	0	0	0	0	0	0	0	0
o_Choreotrichida_ASV_922 -	0	0	0	0	0	0	0	0
Leegaardiella -	7	18	29	30	44	30	29	28
Leegaardiellidae_A_X -	0	0	0	0	0	1	1	1
Discotricha -	0	0	0	0	0	0	0	0
f_Colpodea_XX_ASV_1712 -	0	0	0	0	0	0	0	0
c_Colpodea_ASV_3336 -	0	0	0	0	0	0	0	0
d_Ciliophora_ASV_379 -	0	0	4	2	2	0	0	0
Halteria -	0	0	0	0	0	0	0	0
Hypotrichia_XX -	2	0	0	0	0	0	0	2
Aspidisca -	0	0	0	0	0	0	0	0
Strombididae_B_X -	0	0	1	6	0	1	1	1
Tontoniidae_B_X -	0	0	0	0	0	0	1	0
Pseudotontonia -	2	3	2	0	2	1	9	11
Tontoniidae_A_X -	45	15	0	1	1	1	1	0
Strombidia_C_XX -	0	0	0	2	0	0	0	1
Strombidia_B_XX -	1	3	3	4	1	2	3	3
Strombidium_M -	15	24	36	10	8	12	13	4
Strombidia_F_XX -	0	0	0	0	0	0	0	0
Strombidia_XX -	0	0	0	0	0	0	0	1
Strombididae_G_X -	0	0	1	2	0	1	1	1
Strombididae_H_X -	8	11	11	12	6	11	9	8
Strombidia_G_XX -	0	0	1	1	0	0	0	0
Strombididae_Q_X -	0	0	0	1	1	2	8	1
o_Strombidia_ASV_255 -	0	0	0	0	0	0	0	1
	M2-1 -	M2-2 -	M2-3 -	M1 -	M3-1 -	M3-3 -	M4-1 -	M4-2 -

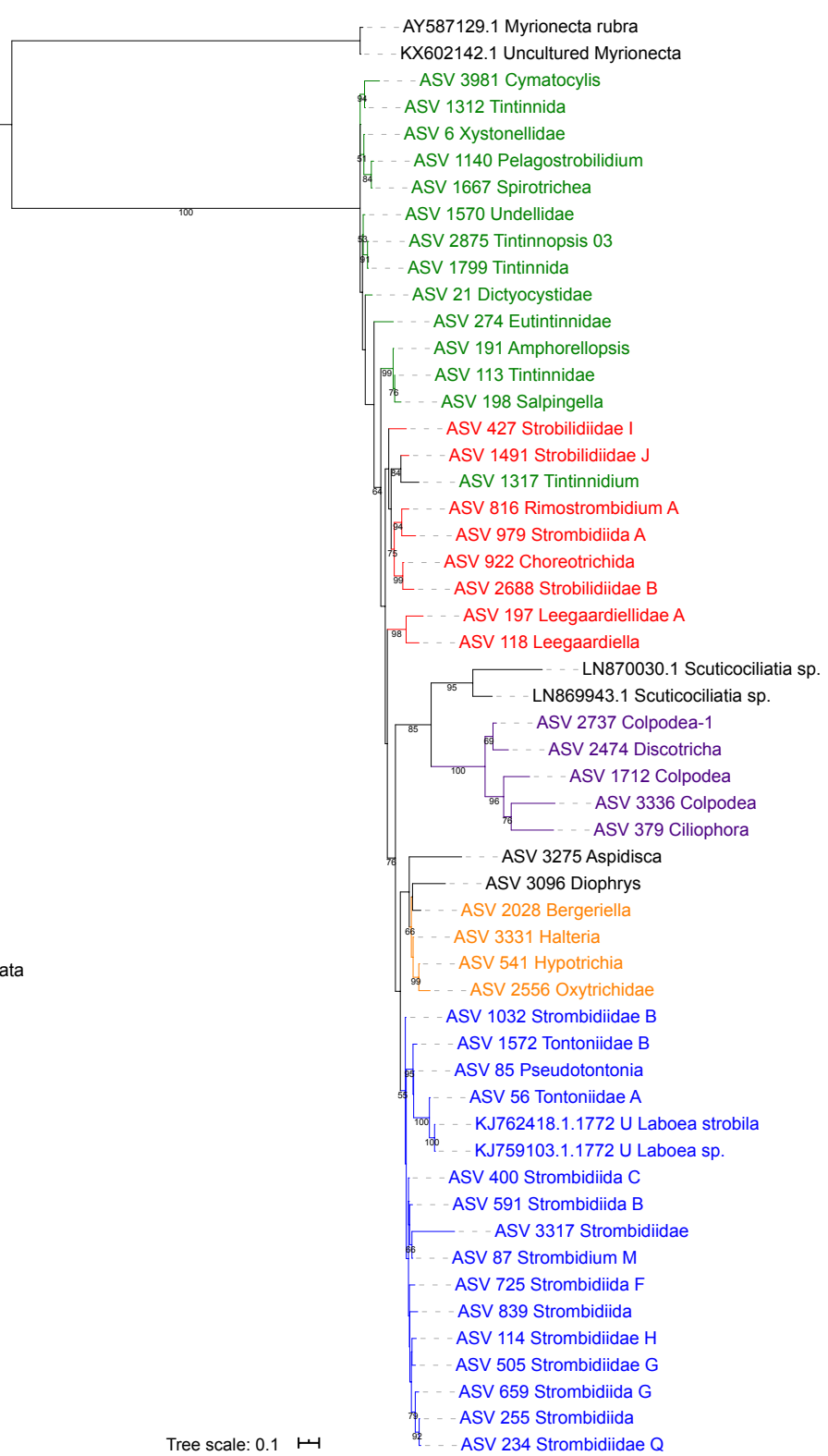
Figure 6

a)



Tree scale: 0.1

b)



Tree scale: 0.1

Figure 7